

This article was downloaded by:

On: 26 January 2011

Access details: *Access Details: Free Access*

Publisher *Taylor & Francis*

Informa Ltd Registered in England and Wales Registered Number: 1072954 Registered office: Mortimer House, 37-41 Mortimer Street, London W1T 3JH, UK



Liquid Crystals

Publication details, including instructions for authors and subscription information:

<http://www.informaworld.com/smpp/title~content=t713926090>

On the structure and the chain conformation of side-chain liquid crystal polymers

L. Noirez^a; P. Keller^a; J. P. Cotton^a

^a Laboratoire Léon Brillouin (CEA-CNRS), CE-Saclay, Gif-sur-Yvette, France

To cite this Article Noirez, L. , Keller, P. and Cotton, J. P.(1995) 'On the structure and the chain conformation of side-chain liquid crystal polymers', *Liquid Crystals*, 18: 1, 129 – 148

To link to this Article: DOI: 10.1080/02678299508036602

URL: <http://dx.doi.org/10.1080/02678299508036602>

PLEASE SCROLL DOWN FOR ARTICLE

Full terms and conditions of use: <http://www.informaworld.com/terms-and-conditions-of-access.pdf>

This article may be used for research, teaching and private study purposes. Any substantial or systematic reproduction, re-distribution, re-selling, loan or sub-licensing, systematic supply or distribution in any form to anyone is expressly forbidden.

The publisher does not give any warranty express or implied or make any representation that the contents will be complete or accurate or up to date. The accuracy of any instructions, formulae and drug doses should be independently verified with primary sources. The publisher shall not be liable for any loss, actions, claims, proceedings, demand or costs or damages whatsoever or howsoever caused arising directly or indirectly in connection with or arising out of the use of this material.

On the structure and the chain conformation of side-chain liquid crystal polymers

by L. NOIREZ*, P. KELLER and J. P. COTTON

Laboratoire Léon Brillouin (CEA-CNRS), CE-Saclay, 91191 Gif-sur-Yvette, France

(Received 14 September 1993; in final form 16 May 1994; accepted 26 May 1994)

Backbone anisotropy and the structure of the mesophases of a series of side-chain liquid crystal polymers have been studied in the bulk by neutron scattering. The backbone conformation is obtained by small-angle neutron scattering on mixtures of hydrogenous polymers with deuterated backbones. The components of the radius of gyration parallel, R_{\parallel} and perpendicular, R_{\perp} to the magnetic field are determined as a function of temperature for both the nematic phase and the smectic phase. It is shown that the polymer backbone is deformed in both phases. When the polymer exhibits only a nematic phase, it adopts a prolate conformation, where the average backbone direction is more or less parallel to the aligned mesogenic groups. Upon transition from the smectic phase to a nematic phase, the backbone in the nematic phase assumes a slightly oblate shape. This tendency towards oblate shape is due to the smectic fluctuations which are always present in such nematic phases. The exentricity of the oblate backbone conformation in the smectic phase is always larger than in the nematic phase. This is attributed to a periodic distribution of the backbone between the mesophase layers. Then, the backbone anisotropy depends not only on the smectic structure (S_{A1} , S_{A2}), but also on the temperature dependence of the density of aligned mesogenic groups in the layers. On the other hand, it is shown that the isotopic mixtures are no longer ideal when polymers deuterated in the mesogenic moieties are mixed with the corresponding hydrogenous polymers.

1. Introduction

Side-chain liquid crystal polymers belong to the large family of high molecular weight materials (called liquid crystal polymers) which present polymorphism. The 'side-chain' term indicates that mesogenic pendants are attached to the linear chain, directly or via a spacer (see figure 1). This architecture resembles a flexible brush or comb, and they are sometimes also called comb-like liquid crystal polymers.

However, it is not essential to graft mesogens onto a linear polymer chain in order to obtain a side-chain liquid

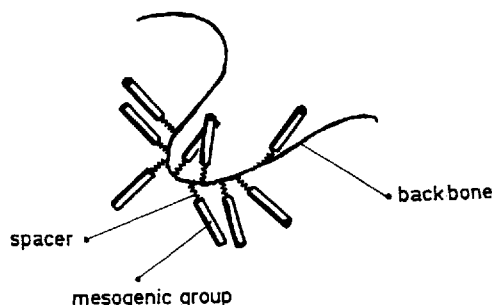


Figure 1. Schematic representation of a side-chain liquid crystal polymer.

crystal polymer. Reciprocally, non-mesogenic side chain monomers can give rise to mesomorphic polymers [1].

The mesophases obtained in the case of liquid crystal polymers are thus a result of a set of interactions involving both the side-chain part and the polymer backbone itself. In this sense, liquid crystal polymers have opened up a new field of investigations. Classical techniques required for understanding the liquid crystal properties (X-ray and SAXS, NMR, optical and electron microscopy, dielectric and acoustic relaxation studies, DSC ...) are of course essential, but are no longer sufficient to investigate these new materials fully, in particular to elucidate the polymer contribution. Neutron scattering is a complementary and powerful method which characterizes both the polymer conformation and the structure of the liquid crystal phase. This method appears to be a unique tool, allowing a description of the evolution of the polymer (its size, its anisotropy obtained at small angles of scattering) in each mesophase as a function of temperature and a simultaneous determination of the mesophase structure (by diffraction at larger angles).

The primary aim of this manuscript is to present as a whole results obtained on such polymers in the bulk by neutron scattering. It will be shown how these results allow one to build a conformational and structural picture

* Author for correspondence.

of the organization of the polymer chain in the smectic and the nematic phases.

The first results obtained in 1985 [2] indicated that the polymer backbone is deformed in liquid crystal phases and led to the following questions: Is this the general case? How does the anisotropy evolve from the isotropic state? Does the backbone or the spacer length play an important role? Is the backbone anisotropy related to the characteristics of the mesophase?

In order to provide answers, a study of a series of side-chain polymers has been undertaken. These polymers involve an acrylate, a methacrylate or a siloxane backbone. In all cases, a calamitic aromatic mesogen is attached as the side-chain via a short polymethylene chain called a spacer.

This paper is divided into two parts (§ 2 and § 3). The first is devoted to a description of the theoretical basis of small-angle neutron scattering (SANS). In particular, the scattering by partially deuteriated liquid crystal polymers is discussed. The experimental procedures are then described.

The second part begins with a systematic presentation of conformational results obtained with a series of liquid crystal polymers. From this presentation, we deduce the general behaviour of the polymer backbone as a function of temperature in each phase (isotropic, nematic and smectic). In the case of nematic phase, we compare the results with various theoretical predictions and propose an explanation for the two shapes (oblate and prolate) obtained in this phase. Similarly, a special section is devoted to the behaviour in the smectic phase. It is demonstrated that the polymer backbone is confined between the liquid crystal layers (oblate shape). An attempt is made to relate the degree of confinement to the stacking of the mesogenic groups in the layers. Finally, we discuss an unusual phenomenon of isotopic segregation between hydrogenous and partially deuteriated polymers (labelled at the extremities of each mesogen unit). We analyse this phenomenon and conclude that it must be limited to particular cases of labelling.

2. Scattering cross-section and experimental method

2.1. Theoretical background

2.1.1. Signal at small-angles and the form factor of polymers

There is one deep relation which connects polymers to neutrons: the coherent neutron scattering at small-angles from which the form factor of the polymer chain [3] can be deduced.

Small-angle neutron scattering (SANS) is due to fluctuations of concentration in the medium. An artificial way to create such fluctuations in bulk (and hence the signal at small-angles) is to mix hydrogenous polymers

with deuteriated polymers [3]. Neutrons directly interact with atomic nuclei and the resulting interaction differs between two isotopes like hydrogen and deuterium, i.e. the coherent scattering length b which characterizes the interaction is -0.374×10^{-12} cm for the hydrogen nucleus $+0.667 \times 10^{-12}$ cm for the deuterium nucleus.

2.1.1.1. Expression of the form factor

The basic formula for interference between pairs i, j of nuclei separated by distance \mathbf{r}_{ij} , associated respectively with the coherent scattering lengths b_i and b_j , is

$$S(\mathbf{q}) = \left\langle \sum_{i,j} b_i b_j \exp(i\mathbf{q} \cdot \mathbf{r}_{ij}) \right\rangle,$$

where \mathbf{q} is the scattering vector ($|\mathbf{q}| = (4\pi/\lambda) \sin(\theta/2)$), θ the scattering angle and λ the wavelength. In the case of N -hydrogenous chains made of n identical repetitive units of z nuclei, each unit is considered as one scatterer of scattering length:

$$a_H = \sum_i^z b_i.$$

$S(\mathbf{q})$ for a mixture of X_H hydrogenous and X_D deuteriated polymers ($X_H + X_D = 1$) can be expressed (in the small q -range of interest, where the size of the repetitive unit is negligible) as

$$S(\mathbf{q}) = X_H X_D (a_H^2 - a_D^2) NP(\mathbf{q}), \quad \text{see [3 (b)].} \quad (1)$$

The form factor $P(\mathbf{q})$ of one chain of n repetitive units can be approximated at small-angles and expressed as a function of its projections over three axes O_x, O_y, O_z : R_x, R_y, R_z :

$$P(\mathbf{q}) = n^2 \langle 1 - (q_x^2 R_x^2 + q_y^2 R_y^2 + q_z^2 R_z^2) \rangle, \quad q_i R_i \leq 1. \quad (2)$$

In the case of liquid crystal polymers with mesogenic groups aligned by a magnetic field, the direction of the field is also a symmetry axis for the polymer anisotropy.

In the following configuration (see figure 2) where the magnetic field and the scattering plane are placed perpendicular to the incident beam, we may measure the scattering intensity in the planes containing the directions parallel and perpendicular to the magnetic field. The measurements allow the determination of two components of the radius of gyration: $R_x = R_{\parallel}$ and $R_y = R_{\perp}$.

2.1.2. Small-angle neutron scattering by partially labelled polymers

In most of the polymers investigated, only the backbone has been deuteriated. It is necessary to know how to interpret the scattering corresponding to a mixture of hydrogenous polymers with partially deuteriated polymers. In particular, it is of interest to check if the partially deuteriated polymer itself produces a signal like the so-called correlation hole [4].

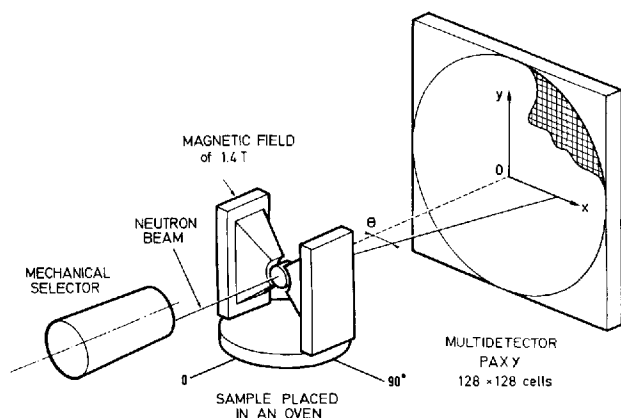


Figure 2. Schematic representation of the SANS device PAXY (Réacteur Orphée) equipped for the study of liquid crystal polymers. The mechanical selector selects the wavelength (usually 10 to 15 Å). The incident beam crosses the sample placed in an oven and between the poles of a magnet whose field is perpendicular to the incident beam. The scattered beam is then collected on the plane of the multidetector.

We suggest an experimental answer: This problem will be analysed first simply by considering the side-chain polymer as consisting of two classes of scatterers: those of the main-chain (backbone) of average coherent scattering length a_1 and those of the side-chain part of average coherent scattering length a_2 .

The associated scattering has been calculated and corresponds to the expression:

$$S(\mathbf{q}, (a_H, a_D), a_2) = \phi(1 - \phi)(a_H - a_D)^2 NP_1(\mathbf{q}) + S_0(\mathbf{q}, (a_H, a_D), a_2), \quad (3)$$

where $P_1(\mathbf{q})$ is the partial form factor associated with the backbone alone.

Experimentally, we demonstrate that the second term S_0 is negligible compared to the first one. Indeed, if we annihilate the first term by taking either an all-hydrogenous sample ($\phi = 1$) or a sample of polymers full deuteriated in the backbone ($\phi = 0$), we measure only the contribution of S_0 to the scattering. The experiment does not show any coherent scattering in the small q -range ($|q|R > 0.18 \text{ \AA}^{-1}$) under these two conditions (see figure 3). The same observation is made in the case of liquid crystal polymers deuteriated, this time, only at the extremity of each mesogenic moiety (absence of coherent scattering see figure 4). The reason why the function $S_0(\mathbf{q})$ corresponds to negligible values probably derives from the strong coupling which exists between the H and D parts of the partially labelled polymer. Indeed, no concentration fluctuations of the H part relative to the D part are allowed in the case of strong coupling and thus, the set of these two labelled and unlabelled elements can then be considered as a single scatterer.

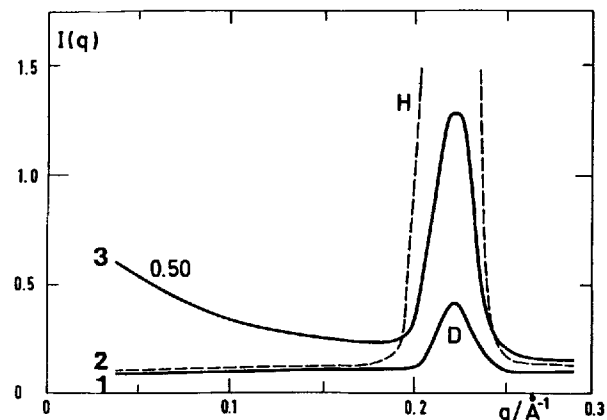


Figure 3. Intensity scattered by a sample containing X per cent of PMA-OC₄H₉ and $(1 - X)$ per cent of PMA(D)-OC₄H₉ in the smectic phase. The direction of observation is parallel to the magnetic field (presence of the 001 reflection at $q = 0.22 \text{ \AA}^{-1}$). Curve (1) corresponds to the polymer deuteriated in the backbone 100 per cent D ($X = 0$). Curve (2) corresponds to the fully hydrogenous polymer $X = 100$. Curve (3) is the H/D mixture of each of the polymers $X = 50$.

The absence of the contribution of S_0 has the consequence that the scattering intensity $S(\mathbf{q}, (a_H, a_D), a_2)$ corresponds to the form factor of the labelled parts of the molecule $P_1(\mathbf{q})$. This intensity is highest with a concentration $\phi = 50$ per cent. This is the value used for all our studies. It has been checked elsewhere that the measured values of the radius of gyration are independent of the concentration ϕ [2(b)].

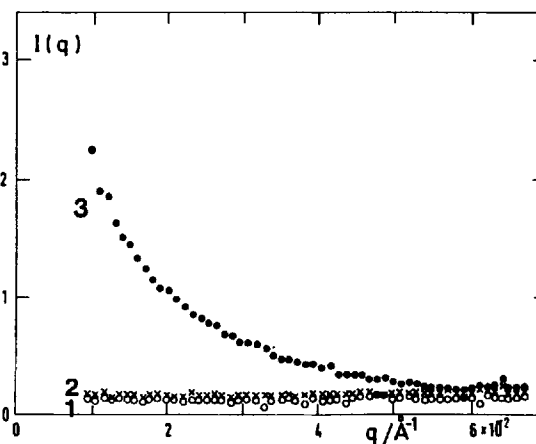


Figure 4. Intensities scattered by the same sample as before but deuteriated at the tail of each mesogenic unit: $(1 - X)$ per cent PMA-OC₄D₉ + X per cent PMA-OC₄H₉. This scattering has been measured for the isotropic phase. Curve (1) $X = 0$, curve (2) $X = 100$, curve (3) $X = 50$.

2.2. Experimental procedures

2.2.1. Determination of R_{\parallel} and R_{\perp} from the raw data

The scattered beam is collected on the plane of a multidetector (PAXY, Lab, Léon Brillouin, Orphée Reactor) made of a network of 128×128 cells of $5 \times 5 \text{ mm}^2$ size [5]. In order to obtain R_{\parallel} and R_{\perp} , one divides the multidetector into 2 rectangular strips (horizontal and vertical) centred on the direct beam. The points in each strip are gathered together as a function of q_{\parallel} and q_{\perp} . The range of q usually chosen is between 0.008 \AA^{-1} and 0.1 \AA^{-1} for a sample–multidetector distance of 2 m and a wavelength of 15 or 10 \AA .

The distance between sample and multidetector enables observation of the 001 reflection of the smectic phase for most of the polymers studied (usually around 25–30 \AA of layer thickness). This is performed simply by switching the wavelength down to 3.7 \AA and keeping the same sample environment.

In order to obtain R_{\parallel} and R_{\perp} , we use a standard procedure (for example see [6]) which can be summarized as follows:

- (i) The background noise is eliminated by subtracting the 1/2 sum of the intensities scattered by a sample containing hydrogenous polymers and another one containing partially deuterated polymers.
- (ii) the efficiency of the cells of the multidetector are normalized by dividing the intensity of each one by the intensity of an incoherent scatterer. The resulting intensity is proportional to the form factor. It can be written, as long as $|\mathbf{q}|R < 2$ in the Guinier range:

in the direction parallel to the magnetic field

$$\frac{1}{I_{\parallel}} \propto \frac{1}{n^2} (1 + q_{\parallel}^2 R_{\parallel}^2),$$

in the direction perpendicular to the magnetic field

$$\frac{1}{I_{\perp}} \propto \frac{1}{n^2} (1 + q_{\perp}^2 R_{\perp}^2).$$

R_{\parallel}^2 and R_{\perp}^2 correspond to the slope at small q -values when one plots the inverse of the intensity as a function of q_{\parallel}^2 and q_{\perp}^2 (Zimm representation).

2.2.2. The sample conditioning

The bulk polymer is placed between two quartz windows of 15 mm diameter spaced by 1 mm. This disk-like cell is put in an oven, itself placed between the poles of a magnet (see figure 2). The thermal process is particularly important, since the physical and mechanical properties of the polymers are very dependent on thermal history. We take this into account by giving a similar thermal history to all the samples. The sample is first heated to the isotropic phase in order to cancel not only the usual polymer memory effects [7], but also the liquid crystal order effect.

The study starts by the determination of R_{\parallel} and R_{\perp} in the isotropic phases and carries on with slowly decreasing temperature ($< 5^{\circ}\text{C h}^{-1}$) of the sample under a magnetic field of 1.4 T. R_{\parallel} and R_{\perp} are then measured at several temperatures in each phase. We check that the polymer has reached an equilibrium state by measuring R_{\parallel} and R_{\perp} several times at a given temperature. The time necessary for one measurement varies from 3 to 20 h. This depends of course on the incident neutron flux and on the polymerization degree (equation (1)), as well as on the contrast density $((a_{\text{H}} - a_{\text{D}})^2)$, see equation (3) between the deuterated and hydrogenous molecules. This is one of the reasons why the error bars on R_{\parallel} and R_{\perp} vary from one polymer to another (see figure 4).

2.2.3. Control of the phase

The nematic phase. By decreasing the temperature from the isotropic phase, the nematic phase appears with an abrupt decrease of transparency at the isotropic–nematic transition. (This eye-control permits one to obtain the transition temperature to around 2–3°).

The smectic phase. The temperature of the nematic–smectic transition in the experiment is then deduced from the value of the isotropic–nematic transition knowing the transition temperatures for each phase from DSC measurements (differential scanning calorimetry). The establishment of the smectic phase is also checked *in situ* by switching down the wavelength to obtain higher values of the scattering vector q and by detecting the presence of the smectic reflection. The quality of the smectic order can be also checked from the width of the smectic peak.

3. Experimental results

This part begins with a description of the characteristics of a list of polymers. The dimensions of the polymers are obtained by SANS from samples aligned in a magnetic field. This list is not exhaustive. In particular, one can note the work of Kalus *et al.* [8], on the conformation of LC polysiloxanes and the results obtained by Mitchell *et al.* [9], on the backbone deformation of LC elastomers by stretching.





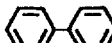
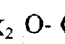
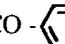
3.1. Description of the series of LC polymers studied

Eight species of polymer have been selected. They can be gathered into three families: (i) the polyacrylates, (ii) the polymethacrylates [10] and (iii) the poly(methylsiloxanes) [11].

The first two classes of polymers have been synthesized by radical polymerization of the side-chain monomers [8], whereas the poly(methylsiloxanes) were obtained by substitution of the hydrogens of a polyhydrogenmethylsiloxane chain by the liquid crystal moieties [9].

The chemical structures of the different polymers are summarized in table 1.

Table 1 List and structural description of the liquid crystal polymers presented in this study.

Polymer	Name	Backbone	Spacer	Rigid core	End of the Mesogenic group
Polymethacrylates	PMA-OC ₄ H ₉	$CX_2-C \begin{matrix} /CX_3 \\ \backslash CO_2 \end{matrix}$	(CH ₂) ₆	O-  -CO ₂ - 	OC ₄ H ₉
	PMA-CN	<i>id.</i>	<i>id.</i>	<i>id.</i>	CN
	PMA-OCH ₃	<i>id.</i>	<i>id.</i>	<i>id.</i>	OCH ₃
Polyacrylates	PA-OCH ₃	<i>id.</i>	<i>id.</i>	<i>id.</i>	OCH ₃
	PA ₆ -CN	<i>id.</i>	<i>id.</i>		CN
	PA ₄ -CN	<i>id.</i>	(CH ₂) ₄		CN
	PA ₅ -OCH ₃	<i>id.</i>	(CH ₂) ₅		OCH ₃
Poly(methylsiloxane)	PMS		(CH ₂) ₃ -CX ₂	O-  -OCO- 	OCX ₃

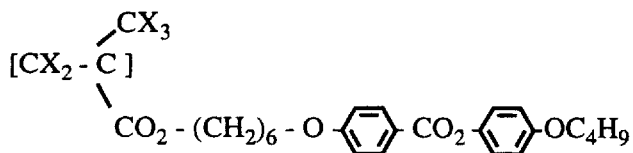
3.1.1. Raw results

A systematic description of the conformation versus temperature is given for each polymer in the following synoptic tables which are not indispensable for an understanding of the subsequent text. Seven polyacrylates and polymethacrylates have been investigated. Since the polyacrylates and the polymethacrylates are deuteriated on the backbone, the components R_{\parallel} and R_{\perp} correspond to the size of the polyacrylate and polymethacrylate backbones, respectively.

On the other hand, different sites of labelling (at the extremity of the mesogenic unit, on the spacer) and two degrees of polymerization have been studied for one type of polymethylsiloxane.

3.2. Backbone conformation of a series of polyacrylates and polymethacrylates from the isotropic phase to the glassy state

The first polymer PMA-OC₄H₉ [2 (b)] corresponds to the following formula:



where $X = H$ or D . It has an averaged weight degree of polymerization, $DP_w \approx 680$ with a polydispersity, $I \approx 3.3$. These averages have been calculated taking into account the hydrogenous polymer and the polymer deuteriated on the backbone, and the polydispersity of each of these. It presents the following succession

of phases:

T_g (glass transition) 38°C S_{A1} 105°C N 110°C I.

PMA-OC₄H₉ presents a narrow nematic temperature range ($\sim 5^\circ\text{C}$) and a broad monolayer smectic phase (S_{A1}). The smectic layer thickness has the same value as the most elongated form of the mesogenic group (29 Å). The variation of R_{\parallel} and R_{\perp} is shown in figure 5.

In the nematic phase, the values of R_{\parallel} and R_{\perp} ($60 \pm 3 \text{ \AA}$ and $65 \pm 3 \text{ \AA}$, respectively) indicate that the polymer backbone adopts a slightly oblate shape (since $R_{\perp} > R_{\parallel}$).

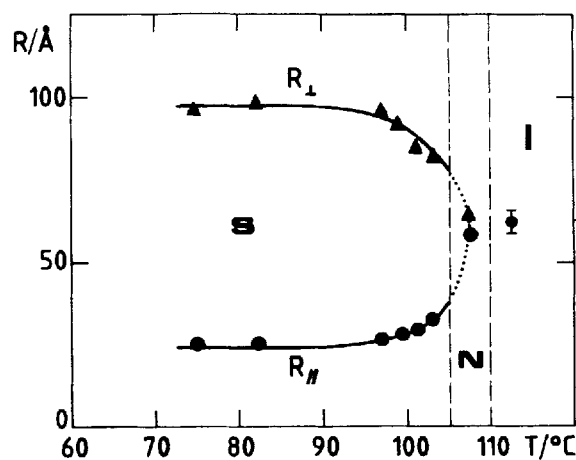


Figure 5. R_{\parallel} and R_{\perp} as a function of temperature for polymer PMA-OC₄H₉.

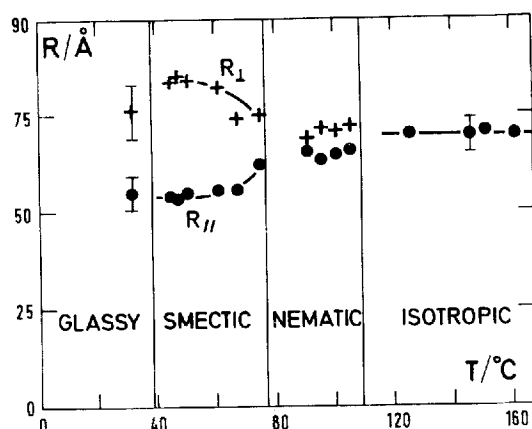
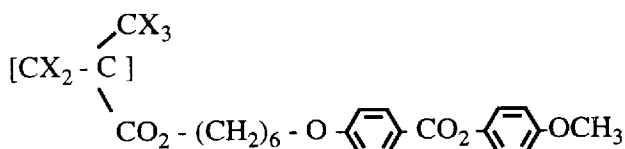


Figure 6. R_{\parallel} and R_{\perp} as a function of temperature for polymer PMA-OCH₃.

In the smectic phase, there is an increase in R_{\perp} and a simultaneous decrease in R_{\parallel} when the temperature decreases. These changes occur over a range of 10°C below the nematic-smectic transition, beyond R_{\parallel} and R_{\perp} keep constant values.

One notices that the error bars are larger for R_{\perp} than for R_{\parallel} . This difference arises from the width of the Guinier domain, which is smaller in the direction perpendicular to the magnetic field than in the parallel direction, and therefore the determination of R_{\perp} is made on a smaller number of points than for R_{\parallel} .

The second polymer, PMA-OCH₃ has the following formula:



where $X = \text{H}$ or D , with a degree of polymerization, $DP_w \approx 800$ and a polydispersity of 2.7.

The succession of phases is:

$$T_g \ 39^\circ\text{C} \ S_{A_1} \ 75^\circ\text{C} \ N \ 108^\circ\text{C} \ I.$$

The only difference between PMA-OCH₃ and the PMA-OC₄H₉ lies in the terminal group -OC₄H₉ or -OCH₃. This change produces a broadening of the nematic temperature range (35°C). At a lower temperature, a smectic phase appears, although it has not always been identified in the literature [2 (a)]. The layer thickness is $25 \pm 1 \text{ \AA}$ which is also the length of the mesogenic group in its extended form (S_{A_1}). Figure 6 gives the variation of R_{\parallel} and R_{\perp} in each phase as a function of the temperature.

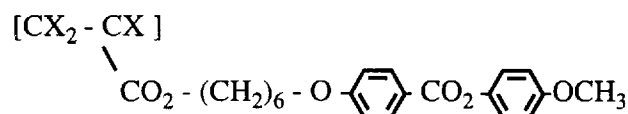
In the nematic phase, R_{\parallel} becomes smaller than in the isotropic phase, whereas R_{\perp} keeps a similar value. This

oblate deformation remains slight over the entire nematic range.

In the smectic phase, the increase in R_{\perp} and the decrease in R_{\parallel} are similar to those obtained in the case of PMA-OC₄H₉ when the temperature decreases, but the anisotropy remains less strong than in the first case.

In the glassy state, the intensity is decreased by a parasitic scattering probably due to the fact that the sample fissures and detaches itself from the windows of the cell.

The third polymer PA-OCH₃ [12], is a polyacrylate with the following formula:



where $X = \text{H}$ or D . The degree of polymerization of the labelled species, for which R_{\parallel} and R_{\perp} are given, is $DP_w = 100$ and the polydispersity is 2.3. The polymer, presents the following succession of phases:

$$T_g \ 22^\circ\text{C} \ S_{A_1} \ 88^\circ\text{C} \ N \ 116^\circ\text{C} \ I.$$

PA-OCH₃ has the same polymorphism as PMA-OCH₃ and the same smectic monolayer thickness of $25 \pm 1 \text{ \AA}$. The evolution of R_{\parallel} and R_{\perp} is shown in figure 7.

In the nematic phase, the global size of the polymer backbone decreases, since R_{\parallel} decreases markedly, while R_{\perp} remains close to the value adopted in the isotropic phase. This again corresponds to an oblate shape.

In the smectic phase, one has the same anisotropy ($R_{\perp} > R_{\parallel}$), but the evolution of R_{\parallel} and R_{\perp} differs from that observed in the cases of PMA-OCH₃ and PMA-OC₄H₉. Indeed the parallel component R_{\parallel} is extremely small and does not vary, whereas R_{\perp} increases from 21 to 27 Å over the same range of temperature.

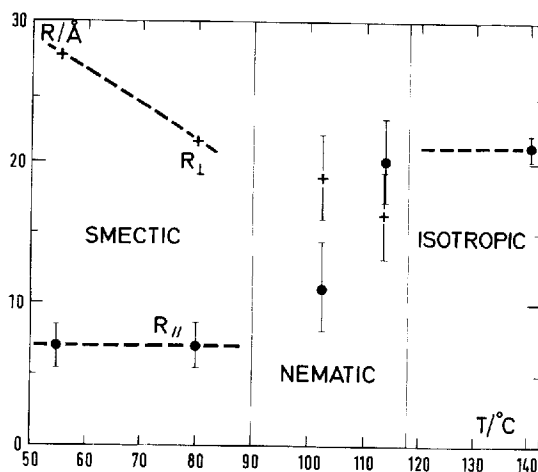


Figure 7. R_{\parallel} and R_{\perp} as a function of temperature for polymer PA-OCH₃.

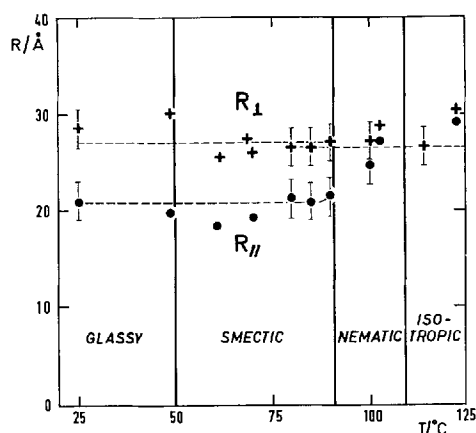
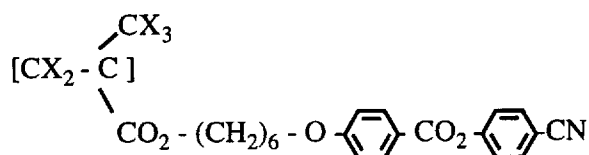


Figure 8. $R_{||}$ and R_{\perp} as a function of temperature for polymer PMA-CA.

The fourth polymer, PMA-CN [13], is a polymethacrylate which differs from PMA-OCH₃ or PMA-OC₄H₉ in having the extremity of the mesogenic group substituted by a cyano group. Its formula is the following:



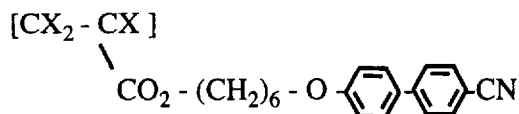
where $X = \text{H}$ or D . The degree of polymerization is $DP_w = 270$ and the polydispersity $I = 2.3$. Its polymorphism is:

$$T_g \ 50^\circ\text{C} \ S_{A_d} \ 92^\circ\text{C} \ N \ 108^\circ\text{C} \ I.$$

The cyano group enhances the polarity of the mesogenic groups and this changes the molecular organization of the smectic phase. It corresponds, in this case, to a partially bilayered smectic phase (S_{A_d} , since the layer thickness ($d = 35 \text{ \AA}$) is larger than the length of the extended mesogenic group (23 \AA), but smaller than twice this length (46 \AA).

Figure 8 shows the values of $R_{||}$ and R_{\perp} in each phase. In the nematic phase, the anisotropy is weak and of the oblate type $R_{\perp} > R_{||}$. In the smectic phase, the difference between R_{\perp} and $R_{||}$ increases with falling temperature, but in contrast to the polymers previously presented, R_{\perp} does not increase, and maintains values close to those obtained for the isotropic phase, whereas $R_{||}$ becomes smaller than in the isotropic phase.

The fifth polymer PA₆-CN [14], has a polyacrylate backbone and the rigid core of the side-groups is constituted by a cyanobiphenyl group, which is therefore different from that in all the preceding polymers. The formula is the following:



where $X = \text{H}$ or D .

The labelled polymer, for which the variation of $R_{||}$ and R_{\perp} is given in figure 9 has a degree of polymerization, $DP_w = 340$ and a polydispersity of 2.3. PA₆-CN presents a special polymorphism:

$$T_g \ 35^\circ\text{C} \ N_{Re} \ 83^\circ\text{C} \ S_{A_d} \ 112^\circ\text{C} \ N \ 122^\circ\text{C} \ I;$$

since a re-entrant nematic phase appears below the smectic phase on decreasing the temperature: the smectic phase is of the S_{A_d} type, since the extended length of the mesogenic group is 23 \AA and the smectic larger thickness is 34 \AA .

In the high temperature nematic phase, the anisotropy corresponds to a weak oblate shape, $R_{\perp} > R_{||}$ despite the error bars. Indeed, the scattering curve shows clearly that the intensity in the perpendicular direction to the magnetic field $I(q_{\perp})$ is always below that of $I(q_{||})$, that is to say $R_{\perp} > R_{||}$. In the smectic phase, $R_{||}$ decreases as the temperature decreases, whereas R_{\perp} keeps a value close to that of the isotropic phase ($52 \pm 2 \text{ \AA}$). The polymer presents then a behaviour similar to that of PMA-CN in the smectic phase. In the re-entrant nematic phase, a striking result is obtained: there is an inversion of the backbone anisotropy which becomes prolate ($R_{||} > R_{\perp}$). Therefore the same polymer can present two types of anisotropy (oblate and prolate) dependent upon the temperature. A discussion about the polymer conformation in the nematic phase will be developed in §3.4.

The sixth polymer, PA₅-OCH₃ [15], is unlike the other polymers in that it possesses only a wide range nematic phase I-N- T_g . It has to the following formula:

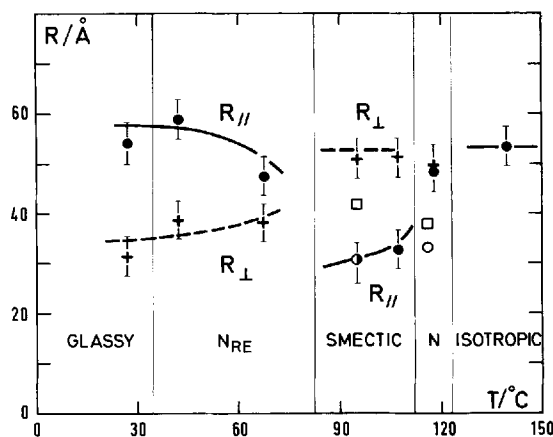


Figure 9. $R_{||}$ and R_{\perp} as a function of temperature for polymer PA₆-CN.

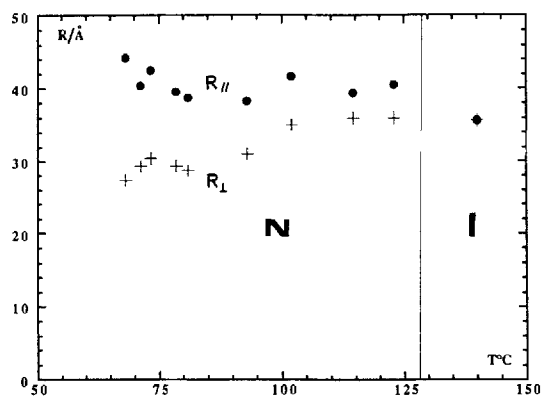
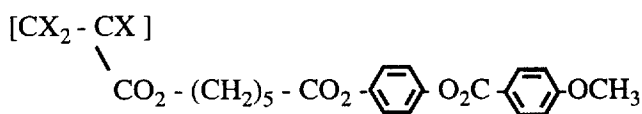


Figure 10. R_{\parallel} and R_{\perp} as a function of temperature for polymer $\text{PA}_5\text{-OCH}_3$.



where $X = \text{H}$ or D .

The polymerization degree of the deuterated polymer, for which the values of R_{\parallel} and R_{\perp} are given in figure 10, is $DP_w = 360$ and the polydispersity is 2.8. The polymer has the polymorphism:

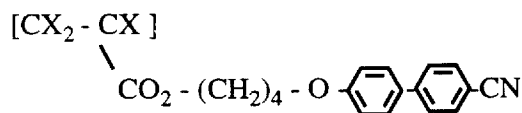
$$T_g \ 50^\circ\text{C} \ \text{N} \ 127^\circ\text{C} \ \text{I.}$$

In the nematic phase, the backbone clearly adopts a prolate shape like PA-CN in the re-entrant nematic phase. Note that the deformation of the backbone begins with an increase of R_{\parallel} whereas R_{\perp} keeps nearly the same value as in the isotropic phase.

The anisotropy and its variation are inverted compared with that for the polymers presenting a smectic phase (R_{\perp} always increases and R_{\parallel} sometimes decreases).

On decreasing the temperature below 65°C , crystallization occurs; this produces an abnormal scattering at very small angles and prevents the determination of the values R_{\parallel} and R_{\perp} in this temperature range.

The seventh polymer, $\text{PA}_4\text{-CN}$, differs from polymer $\text{PA}_6\text{-CN}$ by its spacer length of four (CH_2) instead of six (CH_2). The formula is the following:



where $X = \text{H}$ or D . The phases presented are the following:

$$T_g \ 40^\circ\text{C} \ \text{N} \ 123^\circ\text{C} \ \text{C} \ \text{I.}$$

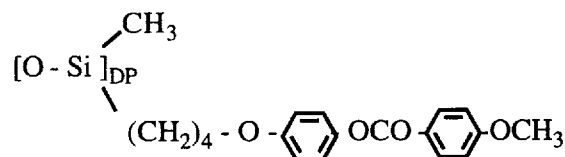
In agreement with Gubina *et al.* [16], this polymer

gives only a nematic phase on cooling the isotropic phase. The polymerization degree is $DP_w \approx 39$ and the polydispersity is 2.7. $\text{PA}_6\text{-CN}$ and $\text{PA}_4\text{-CN}$ correspond to the two sides of the copolymer $\text{PA}_6\text{-CN}/\text{PA}_4\text{-CN}$ [16] where it is shown in a diagram that the re-entrance for $\text{PA}_6\text{-CN}$ disappears as the proportion of $\text{PA}_4\text{-CN}$ increases giving place to a large nematic range. The initial aim was to find, with this polymer, if the inversion of conformation (prolate/oblate) seen in the two nematic phases of $\text{PA}_6\text{-CN}$ occurred also in the broad nematic phase of $\text{PA}_4\text{-CN}$.

Figure 11 shows that the polymer backbone of $\text{PA}_4\text{-CN}$ adopts only a prolate shape over all the nematic range. However, the prolate anisotropy remains weak for about 10°C below the I-N transition and then develops. This variation is still not clearly understood and presents some analogy with the behaviour of $\text{PA}_5\text{-OCH}_3$.

3.3. Conformation of poly(methylsiloxanes)—influence of the labelled site [11]

Collaboration with F. Hardouin-CRPP group of Bordeaux. The liquid crystal poly(methylsiloxanes) called PMS differ from the preceding polymers in their backbone and their shorter spacer (CH_2)₄ directly grafted to the Si atom. The formula of this polymer is



One should note the inversion of the carbonyl group localized between the two phenyl rings. The resulting polymorphism is

$$T_g \ 7^\circ\text{C} \ \text{S}_{Ad} \ 74^\circ\text{C} \ 104^\circ\text{C} \ \text{I.}$$

The smectic phase is partially bilayered (S_{Ad}), since the

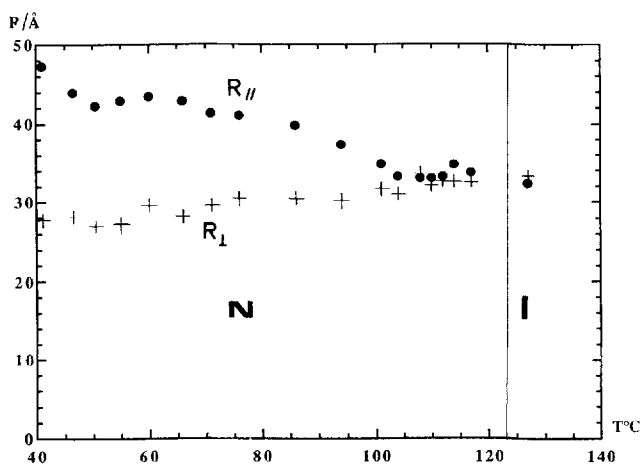


Figure 11. R_{\parallel} and R_{\perp} as a function of temperature for polymer $\text{PA}_4\text{-CN}$.

smectic layer thickness ($d = 36 \pm 1 \text{ \AA}$) remains between once and twice the length of extended mesogenic groups (24 \AA).

The synthesis method (i.e. substitution of some hydrogens from the chain of the poly(hydrogenomethylsiloxane) by mesogenic groups [17]), implies that the labelled part is on the side chain. Two labelling types, (1) at the extremity of each mesogenic unit (OCD_3) and (2) deuteration on the spacer, were used.

The polydispersity is low ($I \approx 1.1$) and two polymerization degrees were chosen ($DP = 35$ and $DP = 80$).

3.3.1. Specific problems for the PMS study

The grafting of the mesogenic units along the poly(methylsiloxane) chain needs a platinum catalyst. Clusters of impurities remain in small quantity in the sample and give rise to a central scattering visible for all the samples (100 per cent hydrogenous, 100 per cent D selectively deuterated, and for the mixture). This disturbs the signal owing to the coherent scattering and also produces a modification of the background level.

Despite the uncertainty about the values of the gyration radii, the type of anisotropy (prolate or oblate) is however clearly determined, since it comes from the direct comparison of the slopes $I^{-1}(q_{\parallel}), I^{-1}(q_{\perp})$ versus $q_{\parallel}^2, q_{\perp}^2$, respectively.

3.3.2. Results obtained with labelling on the extremities of the side-chains

In the case where the mesogenic units are labelled on the extremities ($-\text{OCD}_3$), the SANS signal associated with a mixture of all-hydrogenous polymer with polymer deuterated at the extremities, gives radii of gyration $R_{\parallel g}$ and $R_{\perp g}$ related to the set of these extremities. Since these extremities correspond to the external part of the chain, the scattering intensity gives an overall conformation of the polymer, whereas backbone labelling gives the backbone conformation alone.

3.3.2.1. Influence of the degree of polymerization (DP)

PMS deuterated at the mesogenic group ends of DP = 35 [10]. The values of $R_{\parallel g}$ and $R_{\perp g}$ indicate that overall polymer shape is prolate in the nematic phase as well as in the smectic phase, since $R_{\parallel g} > R_{\perp g}$. It is of interest to know if the *prolate* overall shape is coherent with the *oblate* backbone shape proposed by Kalus *et al.* [8], for a similar PMS of $DP = 63$ labelled on the spacer, since the length of the backbone is of similar size to that of the mesogenic unit. An increase in the polymerization degree should be sufficient to make an inversion of the backbone anisotropy appear.

PMS deuterated at the mesogenic group ends of DP = 80 [11]. This polymer only differs in the polymerization degree ($DP = 80$) and presents the same phase

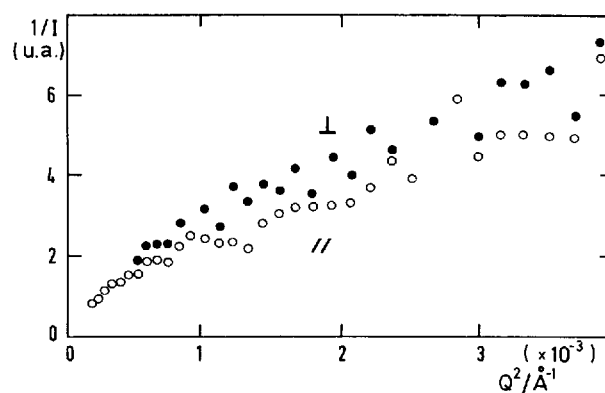


Figure 12. Guinier representation of the intensity scattered parallel and perpendicular in the nematic phase at 85°C for polymer PMS ($DP = 80$) deuterated on the spacer.

succession at the same transition temperatures.

In nematic phase, the overall shape is also prolate, whereas the conformation becomes oblate in the smectic phase and therefore adopts an inverse conformation compared with the polymer of $DP = 35$. The preceding prolate shape observed for $DP = 35$ in fact hides an oblate backbone conformation in the smectic phase.

A rapid estimation of the backbone components R_{\parallel} and R_{\perp} can be deduced from overall measured values by

$$R_{\perp g}^2 = R_{\perp}^2 \quad \text{and} \quad R_{\parallel g}^2 = R_{\parallel}^2 + \langle l \rangle^2,$$

where it is assumed that the nematic order parameter is close to 1 and $\langle l \rangle$, the averaged length of the mesogenic group, is close to 20 \AA . An oblate backbone anisotropy is also deduced in this way from data published for the nematic [10, 11] and this will be experimentally demonstrated with the polymer deuterated on the spacer.

PMS (DP = 80) deuterated on the spacer. The polymer is this time, labelled on the last methylene group of the spacer linked to the rigid core. The polymer shape is then seen from the end of the spacer. Figure 12 gives a Guinier representation of the scattered intensity in the nematic phase at 85°C .

The difference in the slopes shows that the backbone conformation is also oblate in the nematic phase, as found for all the polyacrylates and polymethacrylates having a smectic phase in addition to the nematic phase.

3.3.3. Summary of the different results

In order to analyse the polymer conformation in each mesophase, we shall first recall the behaviour of a polymer in the isotropic phase, in order to discriminate the contribution of the liquid crystal order from that of usual polymer behaviour.

In the case of normal polymers (amorphous), no significant variation of the radius of gyration appears in the bulk state with temperature [3 (b)]. We also found that the

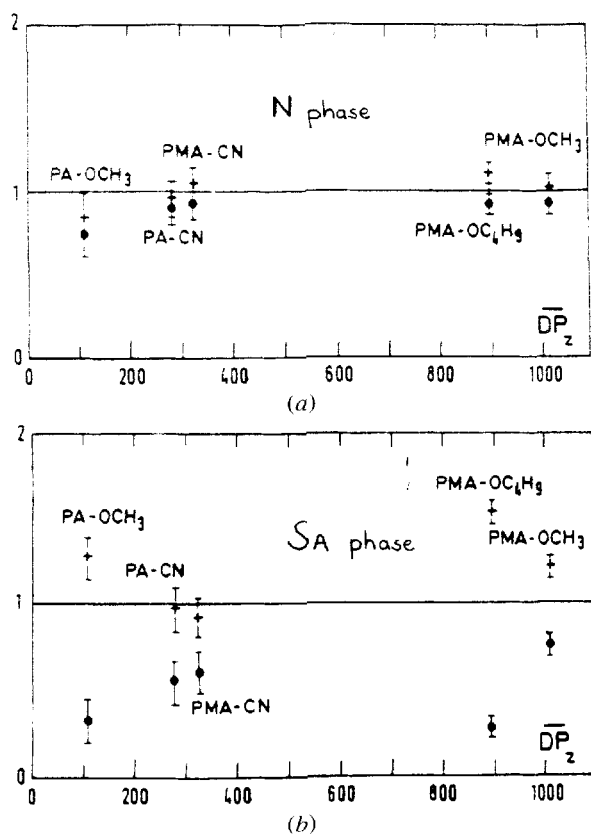


Figure 13. Deformation ratio of the backbone in the smectic phase of different liquid crystal polymers versus polymerization degree. (R_{\parallel}/R_{iso} , ●), (R_{\perp}/R_{iso} , +). (a) In the nematic phase, (b) in the smectic phase.

liquid crystal polymers (PMA-OCH₃) maintain constant sizes in the isotropic phase (within the limit of accuracy of the gyration radius measurement over a range of 40°C).

3.3.3.1. Main results obtained for the nematic and smectic phases

From the study of the different polymers presented, it appears that two types of behaviour can be distinguished: prolate if the mesomorphic polymer possesses only a nematic phase, or oblate when it presents in addition a smectic phase.

The nematic polymer. The first series concerns the polymers PA₅-OCH₃, PA₄-CN and the side-chain copolymer aligned by magnetic field and studied by Mitchell *et al.* [9], which adopt solely a prolate shape over the single large range nematic phase.

The nematic-smectic polymers. The second series includes all the other polymers: the polymethacrylates (PMA-OC₄H₉, PMA-OCH₃, PMA-CN), and the polymethylsiloxanes [11]. Whatever the nematic or smectic phase, the polymer deformation corresponds to the inequality $R_{\parallel} < R_{\perp}$. The backbone tendency is to be

perpendicular to the average direction of the mesogenic groups.

In order to give a general view of the backbone anisotropy of these different polymers, we compare the ratios of R_{\parallel}/R_{iso} and R_{\perp}/R_{iso} , where R_{iso} is the value measured for the isotropic phase.

In the nematic phase, all the polymers presenting a smectic phase, show a small difference ($R_{\perp} - R_{\parallel}$). This difference is always positive, weaker than in the smectic phase and not very sensitive to temperature (see in the preceding section the behaviour of PMA-OCH₃ in the nematic phase). This is shown in figure 13 (a) by the values of R_{\parallel}/R_{iso} , R_{\perp}/R_{iso} very close to the isotropic state: $0.8 < R_{\parallel}/R_{iso} < 1$ and $0.9 < R_{\perp}/R_{iso} < 1.2$.

In the smectic phase, there is a strong deformation of the polymer backbone. It appears that the difference ($R_{\perp} - R_{\parallel}$) increases sharply at the nematic-smectic A transition and over approximately 10°C below this (see, for example, figures 5 or 6). Then R_{\perp} and R_{\parallel} remain almost constant until the glassy state. In figure 13 (b) are reported the values of R_{\perp}/R_{iso} and R_{\parallel}/R_{iso} taken far away from the nematic-smectic transition. It can be seen that the points in the smectic phase are largely more spread around the value 1. Notice that the mosaicity corresponding to the smectic domains keeps constant over the whole temperature range.

Deformation can take place symmetrically in the two directions parallel and perpendicular to the magnetic field (see PMA-OC₄H₉, PMA-OCH₃, PA-OCH₃), but it can also occur only in the direction parallel to the magnetic field (see PA-CN, PMA-CN). In both cases, the parallel dimension of the polymer backbone is always reduced. The smectic phase establishes itself with major rearrangements in the parallel direction which could correspond to a repartitioning of the backbones, mostly between the mesogenic layers.

3.4. Discussion on the nematic phase and the smectic phase

3.4.1. The nematic phase: Confrontation with theoretical models for the nematic phase

One recalls that the two backbone conformations, oblate and prolate, have been found experimentally for the nematic phase. Was theory able to predict these two conformations?

We present here some brief summaries of theories and the limits of their validity (for a more complete description see, for example, [18]).

3.4.1.1. The lattice model adapted for side-chain polymers

Vasilenko *et al.* [19], consider each macromolecule as a succession of n repetitive blocks. The lattice is formed by the set of the N polymers. The partition function Z

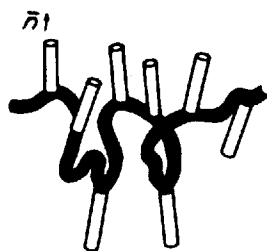


Figure 14. Model proposed for the nematic phase by Vasilenko *et al.* [19].

corresponding to the number of different polymer arrangements in the lattice is calculated, taking into account the fact that the backbone and the spacer are more flexible than the mesogenic group and that they form an angle between them. The minimization of the free energy $\Delta F = -NkT \log Z$ gives different relations between the parameters from which phase diagrams are deduced. There result three oblate conformations. The oblate tendency is more or less important depending on the volume ratio of the backbone sites and the mesogenic unit sites. In the case of the polyacrylates or polymethacrylates studied here, this ratio would be 0.1. Following this theoretical model, the strongest oblate conformation should be obtained when the backbone remains perpendicular to the nematic axis (see figure 14).

This model does not fit the experimental results; moreover it cannot take into account the conformation change with temperature, since the model is built on athermal parameters.

3.4.1.2. A worm-like chain model applied to liquid crystal polymers

Wang and Warner [20] treat side-chain polymer systems by a mean-field model which combines the usual Maier-Saupe theory for the liquid crystal part and the model of worm-like chain for the polymer part. The backbone is considered as a continuous chain where, at each point, a tangent unit vector \mathbf{u} is defined. \mathbf{u} wanders

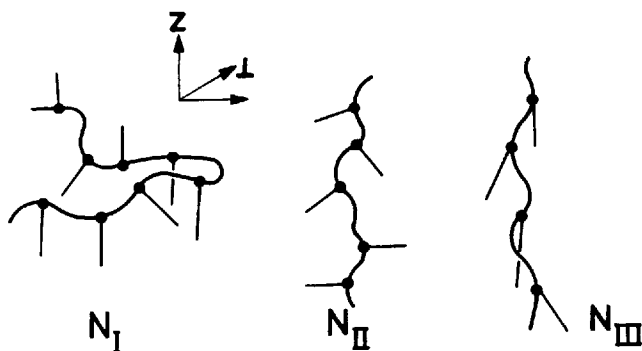


Figure 15. The three backbone conforms predicted by Wang and Warner [20] for the nematic phase.

over the surface of a sphere and is attracted to or repulsed from the poles with a potential U . U contains all the parameters necessary for the description of side-chain polymer systems. Five coupling parameters between mesogenic group, spacer and backbone and two order parameters S_A and S_B are so defined. These last two parameters correspond, respectively to the usual orientational parameter of liquid crystal and a backbone order parameter which gives the type of anisotropy ($S_B > 0$ in the prolate case and $S_B < 0$ for the oblate case). Three backbone conformations called N_I , N_{II} , N_{III} (see figure 15) are deduced, corresponding to different values of the coupling parameters and to the ratio χ of the volume fraction of the mesogenic group on the backbone, and also as a function of temperature.

χ has been calculated in the case of the polymers presented, and gives $\chi > 0.9$. Such a high frequency of mesogenic group repetition along the chain should produce, in all the theoretical cases, an oblate conformation (N_I phase). At present, this theory cannot explain the prolate shape obtained for PA_6-CN , PA_4-CN and PA_5-OCH_3 . Weaker values of χ can account for the two backbone conformations, oblate and prolate, with realistic values of the coupling parameters. A nematic–nematic re-entrance [21] is even predicted, for which the polymer backbone adopts an oblate shape at high temperature and becomes prolate when the temperature decreases. This could correspond to what is observed for PA_6-CN , but no smectic phase is predicted between the two nematic phases. Moreover, the N_I – N_{III} re-entrance is theoretically based on a strong backbone–mesogenic group coupling, which has no physical basis, since the aromatic part of the liquid crystal has no affinity with for the aliphatic part of the backbone.

3.4.1.3. Empirical interpretation of the conformation in the nematic phase

Five oblate shapes and three prolate shapes have been determined. All the polymers presenting an oblate shape form a smectic phase on decreasing the temperature from the nematic phase. Moreover, strong smectic fluctuations [15] or correlation lengths larger or comparable to R_\perp are always detected in the nematic phase. It is then logical to conclude that the oblate backbone conformation could be simply the result of the smectic fluctuations.

In this way, the ‘natural’ conformation adopted by the backbone of a side-chain polymer in a pure nematic phase is a prolate shape. This is in agreement with the structure of the nematic phase which is made of rod-like mesogenic moieties and which sterically favours (if the spacer enables it) a packing of the backbones in the direction parallel to the rod-like units. This prolate shape is relatively independent of the spacer length, since PA_4-CN , PA_6-CN and PA_5-OCH_3 possess different spacers

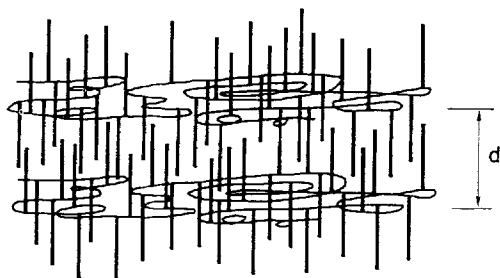


Figure 16. Attempted representation of the polymer backbone confined “quasi-bidimensionally” between layers of liquid crystals.

(respectively, $(\text{CH}_2)_4$, $(\text{CH}_2)_6$ and $(\text{CH}_2)_5\text{-CO}$). The spacer is not short and rigid enough to hold the backbone perpendicular to the liquid crystal part. The same prolate anisotropy has been found for a ‘diluted’ side-chain polymer where the mesogenic units are statistically distributed along a polyacrylate-copolymer [9]. This seems to indicate that the grafting ratio (frequency of mesogenic unit repetition along the backbone) does not influence the anisotropy type. It is also of interest to recall that side-chain liquid crystal polysiloxanes too exhibit a prolate shape in nematic solutions [22]. The prolate shape appears then to be a shape relatively independent of the medium for the nematic phase. This excepts the case of stretched polymers, for which different backbone conformations have been found, depending on the odd or even number of $[\text{CH}_2]$ segments in the spacer [23]. However, we consider here only cases where a magnetic field is applied, and we cannot compare the mechanisms involved in the case of a stretched chain with those for alignment of the side-chain parts by a magnetic field.

3.4.2. Discussion on the polymer conformation in the smectic phase

3.4.2.1. Where is the polymer backbone when the side-chain groups form the smectic arrangement?

From the small-angle neutron scattering data, it appears that the global backbone conformation of the polymer in the smectic phase is oblate ($R_{\parallel} < R_{\perp}$) and becomes more and more oblate when the temperature decreases (see figures 5–11). The component parallel to the magnetic field R_{\parallel} can reach the spectacularly low value of $7 \pm 2 \text{ \AA}$ in the case of PA-OCH_3 (figure 7). The value of R_{\parallel} is smaller than the smectic layer thickness of $25 \pm 1 \text{ \AA}$ (and even half of the layer thickness); the extension of the backbone is not on average sufficient to fill all the thickness of the smectic layer. Since the smectic phase comes from the segregation of the aromatic parts from the aliphatic parts, it can be deduced that the polymer backbone is mostly located between two successive mesogenic layers. The periodic backbone confinement is

also confirmed by the distribution profiles of the backbones which have been determined for a smectic polymer that we could name $\text{PMA-OCH}_6\text{H}_{13}$ [24] and also for $\text{PMA-OC}_4\text{H}_9$ [25]. The case of PA-OCH_3 demonstrates that the backbones, taken as sandwiched between the liquid crystal layers, can be confined quasi-bidimensionally (that is to say on average without crossing through the mesophase layer) between two successive mesogenic layers (see figure 16).

3.4.2.2. Crossing of the backbone through the layers and the parameters for crossing

The polyacrylate PA-OCH_3 corresponds to an extreme confinement with $R_{\parallel} = 7 \pm 2 \text{ \AA}$. All the other polymers studied show values of R_{\parallel} similar to or larger than half of the layer thickness, which implies that on average the backbone does in these cases cross the mesogenic layer (see table 2);

Influence of the polymerization degree. In table 2, one notes that the lowest value of R_{\parallel} (obtained with PA-OCH_3) corresponds also to the lowest polymerization degree. The chain length plays an important role in the mechanism of confinement. The way out of the liquid crystal zones is shorter and easier for a shorter chain. This assumption seems to be checked on comparing the values of R_{\parallel} of PA-OCH_3 to those of PMA-OCH_3 , since these two polymers have the same chemical formula except for the methyl of the backbone. These two compounds also possess the same phase succession and layer thickness ($25 \pm 1 \text{ \AA}$). The high degree of polymerization (~ 700) of PMA-OCH_3 may explain the weak confinement ($R_{\parallel} = 54 \pm 3 \text{ \AA}$) in regard to the strong shrinking of PA-OCH_3 ($R_{\parallel} = 7 \pm 2 \text{ \AA}$).

This result can apparently be extended to the other polymers, if we consider the values of R_{\parallel} and R_{\perp} for the different polymers as a function of z -average of the polymerization degree (since the scattering techniques measure the z -average of R_{\parallel} and R_{\perp} in a case of gaussian polymer [26]). This z -average is deduced from the weight-average by the relation $\langle DP_z \rangle = \sqrt{(2I - 1/I) \times (M_w/m)}$ in the case of Schulz–Flory distribution, where I is the polydispersity and m the molecular weight of the monomer [27]. The values of R_{\parallel} and R_{\perp} versus $\langle DP_z \rangle$ are expressed in figures 17 and 18. The largest values of R_{\perp} correspond to the highest molecular weights. As for R_{\parallel} , the higher R_{\parallel} , the higher is $\langle DP_z \rangle$. The values of R_{\parallel} and R_{\perp} seem then to be related to the chain length. However, no correlation between $(R_{\parallel}, R_{\perp})$ and $\langle DP_z \rangle$ can be established, and other parameters have obviously an influence. For example, the difference between the R_{\parallel} value of $\text{PMA-OC}_4\text{H}_9$ and that of PMA-OCH_3 cannot simply be explained only by the difference between the polymerization degrees.

The dependence of the confinement on the chain length

Table 2. Comparison of physical features of some of the polymers studied.

Polymer	Minimum value of $\langle R_{\parallel} \rangle_z$ / Å	Layer thickness d / Å	Crossing	Polymerization degree in weight	Polydispersity
PA-OCH ₃	7 ± 2	25	no	87	2.3
PMA-OCH ₃	54 ± 3	25	yes	685	2.7
PMA-OC ₄ H ₉	18 ± 1	30	yes	800	3.3
PMA-CN	21 ± 2	35	yes	266	2.4
PA ₆ -CN	30 ± 2	34	yes	340	2.3

raises the problem of thermodynamic equilibrium. It is quite certain that the polymers are in an equilibrium state on the time scale of the experiment (more than five hours) for a given temperature. This is established by the identical results obtained after successive measurements under identical conditions. But kinetic problems could occur when the temperature varies too rapidly, and some definitive knots could occur when the backbone has to cross the backbone interface. It is understandable that the longer the chain, the more numerous will be the entangled knots, and it is most probable that these kinetic defects appear above all during the nematic–smectic transition.

Two kinds of defects can be distinguished.

Existence of kinetic defects. It is shown that the speed with which the temperature is decreased and the time during which the alignment and/or the realignment is carried out in the nematic phase, influences the anisotropy ratio of the polymer backbone. The same sample of PMA-OC₄H₉ is cooled from the isotropic phase, aligned in the nematic phase by a magnetic field of 1.4 T for different alignment times and is then slowly cooled in the smectic phase.

From figure 19, it clearly appears that as the alignment time in the nematic phase increases, R_{\parallel} diminishes and R_{\perp} becomes greater. Since the role of the magnetic field is to reorient the nematic monodomains, the first effect of the

misalignment time is an improvement of the smectic mosaicity. The evaluation of the mosaicity from the 001 Bragg reflections corresponding to curves (1) and (2) shows indeed a shrinking of the Bragg peak width from (1) to (2). However, the variation of R_{\parallel} and R_{\perp} is too large between curves (1) and (2) to be explained only by a better mosaicity (assuming that the backbone layers are tilted with the same angle as the smectic layers, the variation of R_{\parallel} and R_{\perp} between the two alignments should correspond to a very large decrease of the tilt angle of 30° [28]).

The entanglements knots could be understood as a result of the difference in relaxation times between the mesogen and the polymer chain. These times are much slower in the case of the polymer. This interpretation connects with that of Rieger [29] who suggests that these entanglements form at the smectic–nematic transition and no later. In this way, they do not modify the $(R_{\parallel}, R_{\perp})$ curve shape, but the plateau level at low temperature. This seems to be indicated by the similar shape of the three curves in figure 19.

Thermodynamic defects. In contrast with the entanglement knots, some crossings are temperature dependent and give, whatever the thermal history, an analogous decrease in R_{\parallel} (see figure 19). These extensions of the polymer backbone into the liquid crystal layers are called thermodynamic defects.

In the case of PMA-OC₄H₉, the decrease in R_{\parallel} occurs

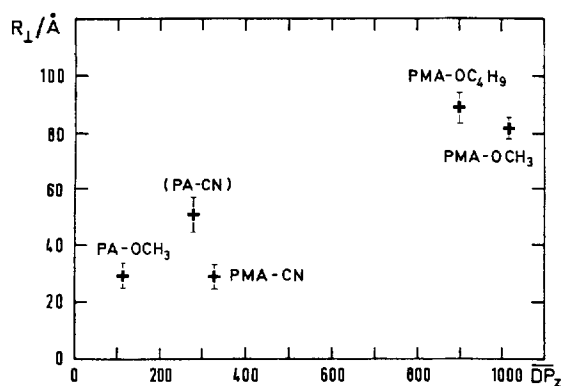


Figure 17. Component R_{\perp} of the backbone gyration radius as a function of the polymerization degree in the smectic phase.

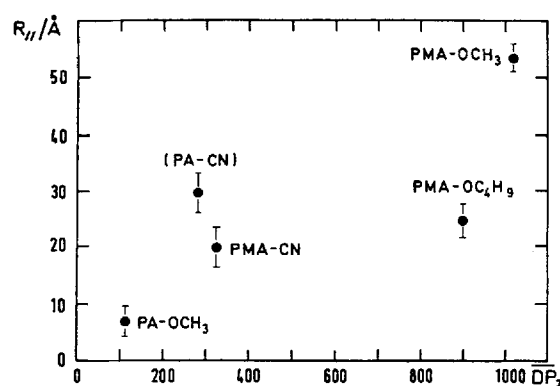


Figure 18. Component R_{\parallel} of the backbone gyration radius as a function of the polymerization degree in the smectic phase.

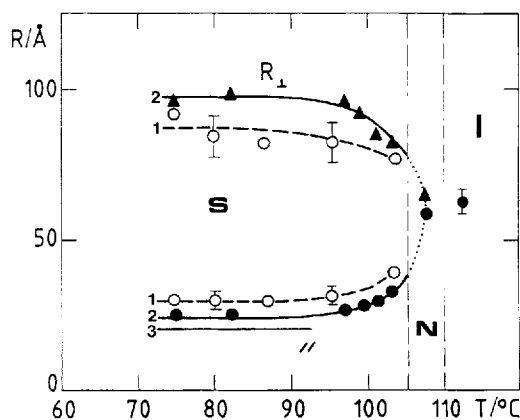


Figure 19. Components parallel R_{\parallel} and perpendicular R_{\perp} to the magnetic field of the gyration radius of the backbone of PMA-OC₄H₉. Curves (1) obtained after an alignment time of $\frac{1}{2}$ hour in the nematic phase. Curves (2) obtained by decreasing the temperature after a rapid reheating of the sample to the isotropic phase, successively to (1), and an alignment time of one hour in the nematic phase. Curve (3) obtained independently from the above two (30 h in the isotropic phase) by decreasing the sample temperature very slowly (1°C/4 h) from the isotropic phase. R_{\perp} is missing, since the experimental conditions could not allow the measurement of both R_{\parallel} and R_{\perp} with good accuracy. Independently of the thermal history, the same value has been obtained ($64 \pm 2 \text{ \AA}$) for the isotropic phase, indicating that there is no polymer degradation. The thermodynamic equilibrium was checked in the smectic phase by repeating twice the measurements of R_{\parallel} and R_{\perp} at one temperature, just above the nematic-smectic transition.

simultaneously with the increase in R_{\perp} when the temperature decreases. Each of these curves can be modelled by a power law. The best accuracy has been obtained with curve (3) [30]:

$$R_{\parallel}(\text{\AA}) = 35(98 - T(^{\circ}\text{C}))^{-0.17 \pm 0.02}$$

where $T = 98^{\circ}\text{C}$ corresponds nearly to the nematic-smectic transition temperature measured under the experimental conditions (this value is relative and averaged, in the sense that it is very difficult to know the temperature inside the sample).

This law has no theoretical basis and is no longer valid at the nematic-smectic transition and at low temperatures. This remark is also true at low and high temperatures for the recent theories presented by Rieger [30] or Renz and Warner [31]. However, the exponential law $\exp(-E/kT)$, where E is a constant and T the temperature, cannot predict the variation of R_{\parallel} and R_{\perp} as a function of temperature. In contrast, the power law found for $R_{\parallel}(T)$ could be directly related to the establishment of the smectic order. Indeed, the smectic order parameter associated with the density of mesogenic units present in the layer can also be expressed as a power law (see for example Brochard [32]). In this way, these 'thermodyn-

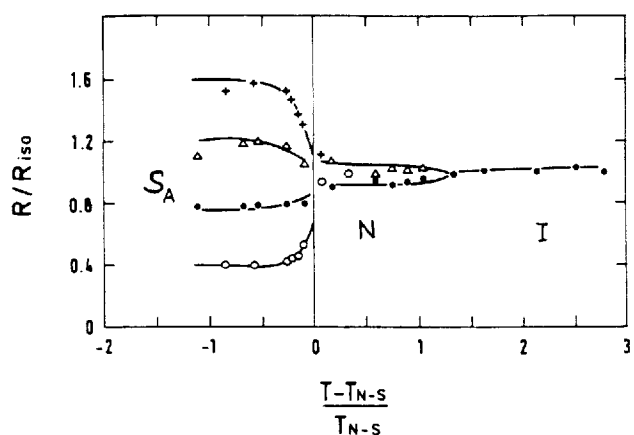


Figure 20. Comparison of the evolution of the reported components R_{\parallel} and R_{\perp} to the values in the isotropic phase ($\sqrt{F(R_{\parallel}; R_{\text{iso}})}, \sqrt{F(R_{\perp}; R_{\text{iso}})}$) for the backbones of PMA-OCH₃ ($R_{\parallel}(\bullet)$, $R_{\perp}(\triangle)$) and PMA-OC₄H₉ ($R_{\parallel}(\circ)$, $R_{\perp}(\text{+})$) as a function of reduced temperature.

amic defects' correspond to allowed extensions of the backbone into the liquid crystal smectic layers. This experimental interpretation will be developed now in the framework of structural (layer characteristics) and conformational (polymer characteristics) results.

3.4.2.3. Structural and conformational comparative analysis of PMA-OCH₃ and PMA-OC₄H₉

PMA-OCH₃ and PMA-OC₄H₉ are two mesomorphic polymethacrylates corresponding to the same chemical formula except for the end of the mesogenic tail which is -OCH₃ for the first polymer and -OC₄H₉ for the second

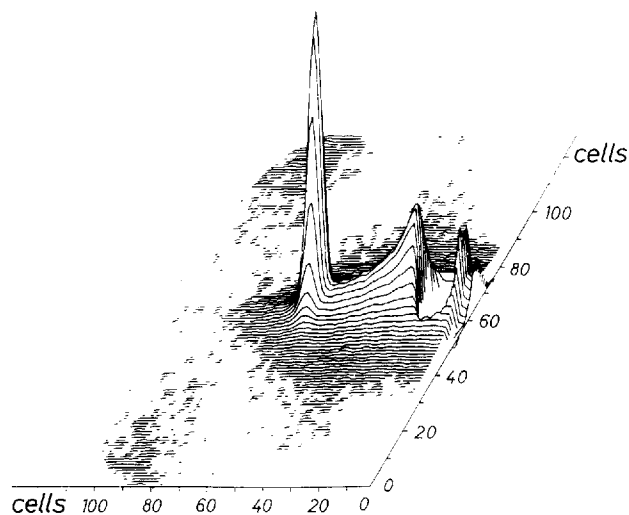


Figure 21. Picture in reciprocal space of the scattering produced by the mixture PMA-OC₄H₉/PMA(D)-OC₄H₉ in the smectic phase ($\lambda = 3.7 \text{ \AA}$, $d = 1.5 \text{ m}$). The small-angle scattering is at the right of the pattern and at the left there is a 001 Bragg reflection of strong intensity.

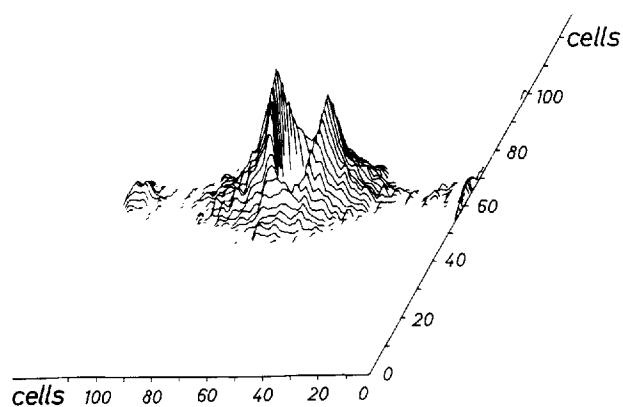


Figure 22. Under the same conditions as fig. 13, the 001 Bragg reflection is of weak intensity in the case of PMA-OCH₃. Here is portrayed the diffraction pattern ($\lambda = 3.7 \text{ \AA}$, $d = 2 \text{ m}$) of the mixture PMA-OCH₃/PMA(D)-OCH₃.

one. They present the same phase succession (S_{A_1} -N-I) and have roughly the same polymerization degree ($DP_w \approx 600$). However, these two polymers present a strong difference in anisotropy (see figure 20).

This difference of anisotropy between PMA-OCH₃ and PMA-OC₄H₉ has to be analysed in terms of alkyl extremity length of the mesogenic unit, since this is the only difference. It is useful then to study the diffraction patterns (neutrons, X-ray) of these polymers in the smectic phase in order to obtain information about the smectic organization.

It appears that whatever the scattering technique used (X-ray or neutrons) and whatever the labelling (5 different labelled species have been considered), the intensity of the 001 reflection of PMA-OC₄H₉ is always stronger than those of the other reflections when they exist, and much more intense than that of PMA-OCH₃, which possesses only the 001 smectic reflection (see figure 21 and figure 22).

In the smectic phase, the density profile (of coherent scattering length or of electronic density) $\rho(z)$ is a periodic function and can be modelled by a Fourier series

$$\rho(z) = \rho_0 + \sum_{i=1}^n F_{00i} \cos\left(\frac{2\pi z}{d} i\right)$$

where $\rho(z)$ is the density at a point on coordinate z along the director, d is the smectic layer thickness and ρ_0 is the average density. The integer n corresponds to the number of smectic reflections ($00i$), since the Fourier transform of $\rho(z)$ produces in reciprocal space an intensity $S(q_z)$

$$S(q_z) \propto \sum_{i=1}^n F_{00i}^2 \delta\left(q(z) - \frac{2\pi z}{d} i\right),$$

where δ is the delta function.

If one assumes now that higher orders are negligible

compared with the 001 Bragg peak intensity, we only have

$$S(q_z) \propto F_{001}^2 \delta\left(q(z) - \frac{2\pi z}{d}\right).$$

The corresponding function $\rho(z)$ in real space is

$$\rho(z) = \rho_0 + \psi \cos\left(\frac{2\pi z}{d}\right)$$

where, following de Gennes [33], ψ is called the smectic order parameter. ψ is proportional to the structure factor $|F_{001}|$. It characterizes the presence probability density of localized mesogenic groups inside the layers. In other words, the higher ψ is, the more the mesogenic groups are localized in the layers and the stronger is the 001 reflection intensity. Finally, although PMA-OCH₃ and PMA-OC₄H₉ are only slightly different, the backbone anisotropy can be explained by a difference in mesogenic group density inside the layers.

From the comparison of the intensities of the 001 Bragg reflection of PMA-OCH₃ and PMA-OC₄H₉, it appears that the layers of PMA-OCH₃ are formed with few localized mesogenic groups inside the layers, whereas many mesogenic groups contribute to the formation of the PMA-OC₄H₉ layers.

The result is that in the first case (PMA-OCH₃), we have an easy crossing of the polymer backbone through the 'soft' liquid crystal layers and a weak backbone anisotropy ($R_{\parallel} \leq R_{\perp}$). In the second case (PMA-OC₄H₉), the polymer backbone cannot extend itself in the direction parallel to the mesogenic groups, since the high mesogen density inside the layers builds a barrier for backbone crossing. There results a strong disymmetry between R_{\parallel} and R_{\perp} , and that means a strong backbone anisotropy.

It is remarkable to see how sensitive the polymer backbone is to the alkyl extremity length, which is a slight modification in a sense where the monolayer structure (S_{A_1}) is maintained. The analysis of the backbone confinement has to be made taking into account the smectic organization. A first approach can be a simultaneous measurement of the backbone anisotropy and the Bragg peak as a function of temperature.

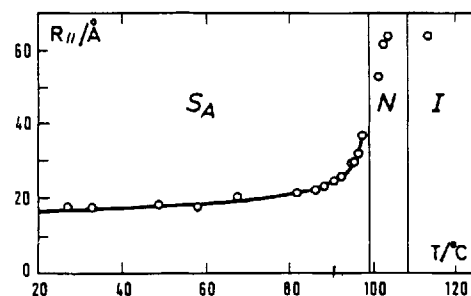


Figure 23. Extension of the polymer backbone in the direction of the mesogenic groups (direction of the magnetic field) versus temperature.

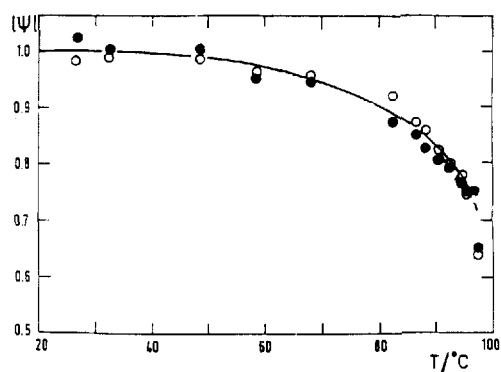


Figure 24. Square root of the integrated intensity representing the smectic order parameter $|\psi|$ versus temperature. The black points correspond to the experimental values measured at the angle $\alpha = 5^\circ$ (●) and the open circles to those measured at $\alpha = 6^\circ$ (○).

3.4.2.4. Evolution of the backbone confinement and of the smectic order parameter as a function of temperature [30]

The extension R_{\parallel} of the backbone along the direction perpendicular to the smectic planes has been measured simultaneously with the integrated intensity of the 001 Bragg reflection, which gives the smectic order parameter Ψ , as a function of temperature (see figures 23 and 24).

These two quantities can be expressed by power laws: $R_{\parallel}(\text{\AA}) = 35(98 - T(^{\circ}\text{C}))^{-0.17 \pm 0.02}$, $\psi = \psi_0 + A(97.3 - T(^{\circ}\text{C}))^{0.3 \pm 0.1}$, $\psi_0 = 0.60 \pm 0.10$ (arbitrary units), $A = 1.10 \pm 0.50$ (arbitrary units).

Although these power laws have no theoretical basis, the complementarity of these two curves shows that there is a direct correspondence between the order of the smectic phase and the confinement of the backbone between the mesophase layers. This analogy can be a starting point for new theories (the previous theories involve an exponential law: $R_{\parallel} \propto \exp(-E/KT)$; E is taken as a constant by Rieger [29] and E as proportional to $\sqrt{\psi}$ by Renz and Warner [31]).

In order to complete this study, the higher orders of smectic reflections (002, 003) have been carefully measured using a neutron diffraction spectrometer [25]. The same procedure as that explained for only one smectic reflection was used in order to reconstruct the profile of coherent scattering length versus temperature for PMA-OC₄H₉ and PMA(D)-OC₄H₉. The subtraction of the respective profiles of these two isotopic species allows the extraction of the profile of the backbones alone inside the mesophase layers. It is so demonstrated that the backbones are all the more concentrated outside the mesogenic side-chain zone as the temperature decreases. Moreover, there is still backbone crossing of the mesophase zone at low temperature. The number of monomers crossing the

mesogenic layer has been evaluated as 25 percent of the set of backbone monomers at low temperature.

3.4.2.5. Influence of the smectic arrangement (S_{A_1} , S_{A_d}) on the backbone conformation

It is remarkable to note (figure 25) that the confinement of the polymer backbone in a S_{A_1} structure (monolayer smectic phase) always produces, in addition to the decrease in R_{\parallel} , an extension of the backbone size between the mesophase layers (R_{\perp} increases) (see figure 5, PMA-OC₄H₉, figure 6, PMA-OC₃, and figure 7 PA-OC₃). Whereas in a S_{A_d} structure (partially bilayered smectic phase with a partial overlap of the mesogenic cores), the backbone is also confined between the layers (R_{\parallel} decreases), R_{\perp} maintains a value close to that of the isotropic phase (see figure 8, PMA-CN, and figure 9, PA₆-CN).

The overlap which characterizes the S_{A_d} phase leads to a less dense mesogenic region compared to that in a S_{A_1} phase. In the S_{A_d} structure, the polymer backbone is generally less compressed sterically and does not need to extend itself in the direction perpendicular to the mesogenic units. This could provide an explanation for the invariance of R_{\perp} from the isotropic phase. This also implies an invariance of the state of conformation (gaussian, excluded volume, ...) of the backbone, in the direction perpendicular to the mesogenic groups, on passing from the isotropic state to the state confined between the liquid crystal layers.

Perspectives. Whatever the smectic arrangement (S_{A_1} , S_{A_d}), the polymer backbone is excluded from the liquid crystal zones (R_{\parallel} decreases) and this results in an increase in R_{\perp} only if the compactness of the smectic phase is high (S_{A_1} phase). In this way, it could be of interest to measure the elastic constants of the smectic layers of the liquid crystal polymer. In particular, measurement of the

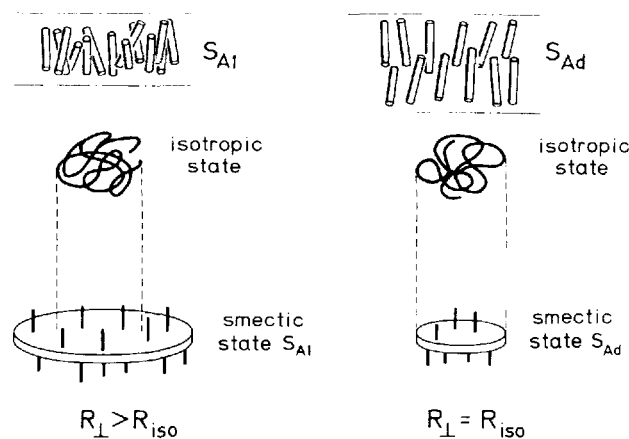


Figure 25. Naïve representation of variation of R_{\parallel} and R_{\perp} in an example of the S_{A_1} phase and of the S_{A_d} phase.

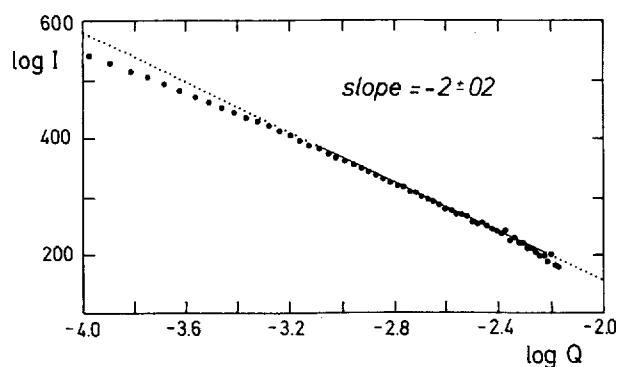


Figure 26. Logarithmic representation of the scattering intensity as a function of the scattering vector q . The slope of the curve is $\alpha = -2.0 \pm 0.2$ for $qR \geq 4$.

elastic compressibility constant for different smectic layers of polymers as a function of temperature could give a quantitative approach to what we have only qualitatively state. This assumption implies that theories based on activation energy are unsuitable.

3.4.2.6. Some indications for the conformation of the polymer backbone between the mesophase layers

What the theory expects. According to the Rieger's predictions [29], the invariance of R_{\perp} from the isotropic phase to the smectic phase traduces a gaussian state (PMA-CN, PA₆-CN) of the backbone between the mesophase layers, whereas a higher value of R_{\perp} (than in the isotropic phase) means that the backbone tends to adopt a rod-like conformation.

The intermediate range of study. The scattering function for $qR \geq 4$ (intermediate range) is often a power law $(I(q))^{-\alpha}$ where the exponent α differs with the shape of the scattering object [34].

The experiment has been carried on with a sample of PMA-OC₄H₉ aligned in the smectic phase in such a way that the normal to the layers is parallel to the incident beam. The results are presented in figure 26 from which one deduces the exponent value $\alpha = 2 \pm 0.2$. The exponent should correspond to a gaussian conformation, but a higher molecular weight has to be studied to widen the intermediate range and to confirm the α value. On the other hand, other objects in 2-dimensions may perhaps also give the same exponent.

3.5. Specific phenomenon of isotropic segregation between liquid crystal polymers

The determination of the polymer conformation in the bulk assumes that the labelled and unlabelled chains are randomly mixed. It is shown here that a segregation occurs when LC polymers deuteriated at the extremities of each mesogenic group are mixed with the hydrogenous analogues. This leads to aggregation between scatterers of the

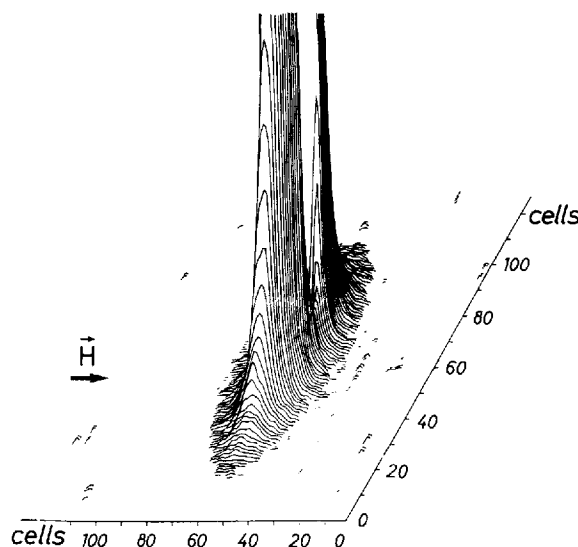


Figure 27. Very strong anisotropic signal obtained at small angles ($\lambda = 15 \text{ \AA}$, $d = 2 \text{ m}$) for the mixture PMA-OC₄H₉/PMA-OC₄D₉ in the smectic phase.

same isotopic species and forms objects of considerable sizes. The phenomenon is particularly surprising [35] on account of the weak number of deuteriated atoms and the low degree of polymerization ($DP_w \approx 600$).

3.5.1. Abnormal small-angle scattering

As soon as the scatterer size greatly exceeds the value corresponding to the inverse of the minimum of $|\mathbf{q}|$ (the limit-value measurable $\sim 500 \text{ \AA}$ for the SANS-device PAXY), the Porod regime is reached and the scattered intensity can be modelled by a q^{-4} power law.

Such a scattering has been identified for a mixture of PMA-OC₄H₉ with its analogue deuteriated at the extremities of each mesogen (-OC₄D₉). This scattering occurs *as soon as the smectic phase appears* on decreasing the temperature from the isotropic phase. The pure compounds (100 per cent hydrogenous PMA-OC₄H₉ or 100 per cent deuteriated PMA-OC₄D₉) do not give any signal under identical conditions. Moreover, the strong scattering obtained for the H/D mixture is anisotropic (see figure 27) (it is recalled that the sample is held in a magnetic field). A study at very small angles $\lambda = 15 \text{ \AA}$, $d = 7 \text{ m}$) shows that the intensity of the signal follows a power law in $1/q^4$ both in the parallel and perpendicular directions. The intensity should vary more rapidly in the direction parallel to the magnetic field if one considers that the majority of the parallel signal falls inside the beam trap (even at the limit conditions $\lambda = 15 \text{ \AA}$, $d = 7 \text{ m}$). The scattering anisotropic object is oriented with the long axis parallel to the magnetic field.

It is of interest to follow the formation of this object in the nematic phase. Indeed, this phenomenon begins early

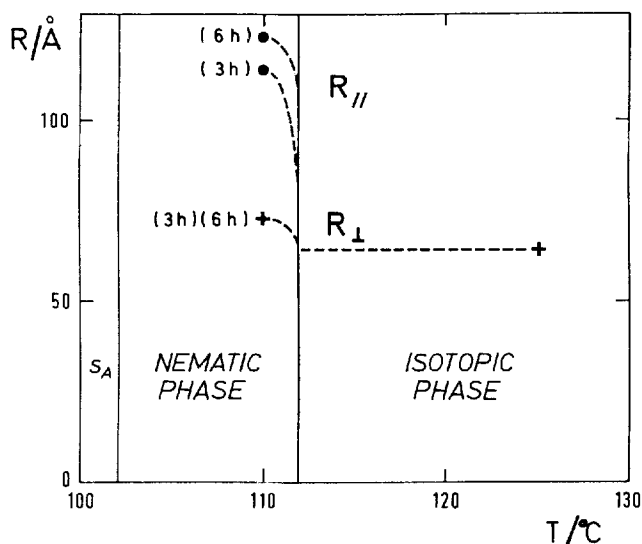


Figure 28. Variation of the values of $R_{//}$ and R_{\perp} determined in the case of the mixture PMA-OC₄H₉/PMA-OC₄D₉ as a function of time.

in the nematic phase according to the abnormal evolution in time of the components $R_{//}$ and R_{\perp} of the radius of gyration (see figure 28). In the isotropic phase, no anisotropy is detected. Just after the nematic–isotropic transition, the anisotropy appears with $R_{//} > R_{\perp}$. $R_{//}$ increases as a function of time indicating that an object is beginning to form itself by stretching out in the direction parallel to the magnetic field.

On decreasing the temperature, a very strong and intense central scattering appears as soon as the nematic–smectic transition occurs. The small-angle coherent scattering is substituted by a q^{-4} power law, and so the gyration radius cannot be determined.

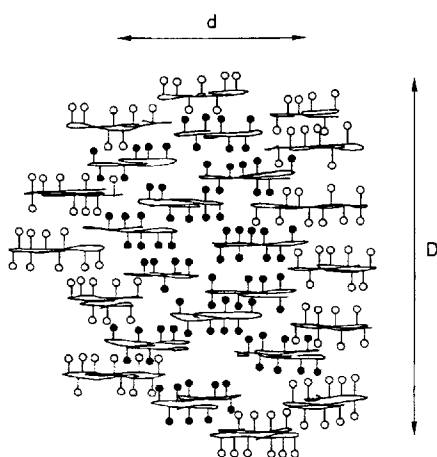


Figure 29. Attempted representation of smectic columns of the same isotopic species.

3.5.2. Analysis of the phenomenon and comments

The abnormal central scattering observed in the smectic phase has been attributed to a phenomenon of aggregation between polymer molecules of the same labelling. This assumption is supported by the X-ray study at small angles of each isotopic species. Indeed, no difference has been detected between the scattering produced by the pure compounds (100 per cent PMA-OC₄H₉, 100 per cent D PMA-OC₄D₉) and the mixture (50/50 PMA-OC₄H₉/PMA-OC₄D₉). This result is compatible with an isotopic segregation which is invisible for X-ray scattering, since hydrogen and deuterium are identical from an electronic point of view.

A microscopic interpretation of this phenomenon could be the formation of long columns containing polymer molecules of the same isotopic species (see figure 29). This segregation is superimposed on the smectic order, since the fineness of the Bragg peak and the sample transparency indicate that the mesogenic units are aligned in the magnetic field direction. The segregation progress (formation of the columns) and the formation of the smectic layers occur simultaneously. The speed with which the segregation takes place gives an idea of the chain mobility and of its range. It is also of interest to note that the segregation only appears with polymers deuteriated at the extremities. Some conclusions could be drawn from these observations. This segregation must be strongly related to the interactions between mesogenic groups, particularly in the smectic phase (it is here demonstrated how much the tails play an important role). Indeed, the smectic arrangement does increase the short range interactions between mesogens, and it has also been shown [36] that the mesophase stability is strongly dependent on the interactions between mesogen extremities.

On another hand, the mixture PMA-OC₄H₉/PMA-OC₄D₉ gives rise to an additional bump located on the meridian and corresponding approximately to a double smectic period. The origin of this bump is not yet clearly understood and other studies need to be performed to understand the relations between the segregation mechanism and the resulting structure of the LC polymer.

Finally, one recalls that no abnormal scattering has been detected when the mixture is made with hydrogenous polymer and polymer deuteriated in the backbone instead of in the extremity. This mixture gives the usual behaviour of isotopic mixtures. It is thereby demonstrated that the isotopic nature of the backbone has no direct influence on the mesophase stability.

4. Conclusions

A series of nine side-chain liquid crystal polymers has been chosen in order to determine the influence of the nematic and the smectic organization on the polymer

backbone conformation in the bulk. From this study, general features can be drawn.

(1) In the nematic phase, whatever the polymer backbone (polyacrylate or polymethacrylate), two backbone conformations (oblate, prolate) can be obtained. It clearly appears that all the polymers giving a smectic phase after the nematic phase on decreasing the temperature have in the nematic phase an oblate shape in which the polymer backbone is more or less perpendicular to the orientation of the mesogenic units. Smectic fluctuations, which are associated with the coming smectic phase and are present in the nematic phase have correlation lengths of the same order or higher than the size of the polymer backbone in the nematic phase. The smectic fluctuations induce an oblate backbone conformation which is the characteristic conformation of the backbone in the smectic phase.

Indeed, all the polymers possessing only a nematic phase (without a smectic phase) at low temperature correspond to a prolate conformation in which the average direction of the polymer backbone is the same as the orientation of the mesogenic groups.

The conclusion is that the organization of the nematic phase favours an elongation of the polymer backbone in the direction of the mesogenic units (as long as the spacer length allows it). This situation is sterically the most convenient, since packing is fulfilled simultaneously for the mesogenic groups and the backbone.

(2) In the smectic phase, the backbone conformation is always of an oblate shape for which the average direction of the polymer backbone is perpendicular to the liquid crystal orientation. This oblate anisotropy is always greater than in the preceding nematic phase and increases when the temperature decreases. In some cases, the backbone reaches an anisotropy such that the extension R_{\parallel} in the direction of the mesogenic groups becomes smaller than the smectic layer thickness itself (see the case of PA-OCH₃; $R_{\parallel} = 7 \pm 2 \text{ \AA}$, $d(\text{layer thickness}) = 25 \pm 1 \text{ \AA}$ [27]). It is then highly probable that the polymer backbone is more or less distributed between the neighbouring mesophase layers. The backbone anisotropy detected in the smectic phase can be interpreted by an exclusion of the backbone chain from the mesogenic zones.

PA-OCH₃ could be considered as an exceptional case of confinement, since the backbones are mostly located quasi-bidimensionally between only two successive mesophase layers. The other polymers of higher molecular weight do not present such a confinement, since the R_{\parallel} value indicates that the backbone crosses the layers. Therefore, it seems that the polymerization degree plays an important role in the strong anisotropy of PA-OCH₃.

Independently of the polymerization degree, it appears that the characteristics of the smectic phase control the backbone anisotropy: PMA-OCH₃ and PMA-OC₄H₉

present the monolayer smectic phase (S_{A_1}) and are of identical formulae except for the mesogen extremity (OCH₃ and OC₄H₉). However, in the S_{A_1} phase, PMA-OCH₃ adopts a slightly oblate shape, whereas PMA-OC₄H₉ presents a strongly oblate anisotropy.

It has been shown by X-ray [10] and by neutron scattering that the strong anisotropy of PMA-OC₄H₉ coincides with a high density of mesogenic groups inside the layers (strong 001 Bragg peak intensity) and a better localization of these groups inside the layers (multiplicity of the Bragg orders). It is remarkable to see that such a small change in the extremity length of the liquid crystal group induces such a strong difference in the backbone anisotropy, despite keeping the structure of the smectic phase the same $-S_{A_1}$.

From the simultaneous measurements of R_{\parallel} and the intensity of the 001 Bragg reflection of the polymer PMA-OC₄H₉, it has been qualitatively demonstrated that the more ordered the smectic phase, the more the polymer backbone is located between the mesogenic layers. Indeed, there is a direct correlation between the smectic layer density Ψ (assumed proportional to the square root of the 001 Bragg intensity) and the extension R_{\parallel} (since these two quantities R_{\parallel} and Ψ can be expressed by a power law in which R_{\parallel} decreases when the temperature decreases, whereas Ψ increases).

This experiment shows how much the extension of the polymer backbone in the direction of the axis of the mesogenic groups is conditioned by the number of mesogenic groups which form the layers. The variation of Ψ and R_{\parallel} during the decrease in temperature is also a proof of the mobility of the mesogenic and the backbone parts. These motions take place over a long range, since the length of the spacer (CH₂)₆ does not totally decouple the backbone from the liquid crystal motion.

The type of smectic phase (S_{A_1} , S_{A_d}) has also a strong influence on the backbone behaviour. It seems that in the case of a partially bilayered smectic phase, S_{A_d} , the polymer backbone (PMA-CN, PA₆-CN) does not extend itself in the direction perpendicular to the mesogenic units, keeping the R_{\perp} value of the isotropic phase ($R_{\perp} \approx R_{\text{iso}}$). This is in marked contrast to the strong increase in R_{\perp} always observed for polymers giving a monolayered smectic phase, S_{A_1} (PMA-OCH₃, PA-OCH₃, PMA-OC₄H₉). This difference could be interpreted by the weak compactness of the S_{A_d} phase which reduces sterically the constraints on the backbone which is more or less localised between the mesophase layers.

The study in the intermediate range of scattering in the plane of the smectic layers of PMA-OC₄H₉ gives a scattering type of power law compatible with that which could give a gaussian walk of the backbone between layers. However, the gaussian assumption has to be checked, for example, by the measurement of R_{\perp}

on monodisperse samples of different molecular weights.

Finally, it must be noted that the small-angle scattering, from which R_{\parallel} and R_{\perp} are extracted, is obtained with a mixture of hydrogenous and deuteriated polymers. This mixture is assumed to be ideal. This seems to be correct in the case of deuteriated backbones, but this is no longer the case when the extremities of the mesogenic units are deuteriated. The H/D separation clearly appears as soon as smectic phase occurs; this shows how sensitive this phase is to local interactions, in particular between the mesogenic tails, and how much the deuteration affects the physical (liquid crystal) properties of the liquid crystal polymers. It is certain that many other studies have to be made to understand the isotopic separation phenomenon in liquid crystal polymers systems.

We are very grateful to H. Benoît for his help in the elaboration of the contrast expressions given in § 3.3., to F. Hardouin for collaboration in the study of the liquid crystal polysiloxanes and to C. Taupin and M. Lambert for their interest in this work.

References

- [1] FINKELMANN, H., *Liquid Crystals of One and Two Dimensional Order* (Springer Series in Chemical Physics, **11**, 238.
- [2] (a) KIRSTE, R. G., and OHM, H. G., 1985, *Makromolek. Chem. rap. Commun.*, **6**, 179. (b) KELLER, P., CARVALHO, B., COTTON, J. P., LAMBERT, M., MOUSSA, F., and PÉPY, G., 1985, *J. Phys. Lett.*, **46**, 1065.
- [3] (a) DE GENNES, P. G., 1979, *Scaling Concepts in Polymer Physics* (Cornell University Press). (b) COTTON, J. P., DECKER, D., BENOÎT, H., FARNOUX, B., HIGGINS, J., JANNINK, G., DES CLOIZEAUX, J., OBER, R., and PICOT, C., 1974, *Macromolecules*, **7**, 863. (c) GARVISH, W., BRERETON, M. G., and FISHER, E. W., 1981, *Polymer Bull.*, **4**, 687.
- [4] BOUÉ, F., DAUD, M., NIERLICH, M., WILLIAMS, C., COTTON, J. P., FARNOUX, B., JANNINK, G., BENOÎT, H., DUPLESSIX, R., and PICOT, C., 1978, *IAEA-SM-219*.
- [5] "Equipements Expérimentaux", available at the Lab. Léon Brillouin, CE-Saclay 91191, Gif-sur-Yvette Cédex, France.
- [6] For example, BOUÉ, F., 1982, Ph.D. Thesis, Université Paris-Sud, Orsay (in French).
- [7] KOVACS, A. J., AKLONIS, J. J., HUTCHINSON, J. M., and RAMOS, A. R., 1979, *J. polym. Sci.*, **17**, 1097.
- [8] KALUS, J., KOSTROMIN, S. G., SHIBAIEV, V. P., KUNCHENKO, A. B., OSTANEVICH, D. A., and SVETOGORKY, YU. M., 1988, *Molec. Crystals liq. Crystals*, **155**, 347.
- [9] MITCHELL, G. R., DAVIS, F. J., GUO, W., LYWINSKI, R., 1991, *Polymer*, **32**, 1347.
- [10] (a) PORTUGALL, M., RINGSDORF, H., and ZENTEL, R., 1982, *Makromolek. Chem.*, **183**, 2311; (b) PÉPY, G., NOIREZ, L., KELLER, P., LAMBERT, M., MOUSSA, F., and COTTON, J. P., 1990, *Makromolek. Chem.*, **191**, 1383.
- [11] (a) HARDOUIN, F., NOIREZ, L., KELLER, P., LAMBERT, M., MOUSSA, F., and PÉPY, G., 1988, *Molec. Crystals liq. Crystals*, **155**, 389. (b) MOUSSA, F., COTTON, J. P., HARDOUIN, F., KELLER, P., LAMBERT, M., PÉPY, G., MAUZAC, M., and RICHARD, H., 1987, *J. Phys., France*, **48**, 1079. (c) PÉPY, G., NOIREZ, L., KELLER, P., LAMBERT, M., MOUSSA, F., COTTON, J. P., STRAZIELLE, C., HARDOUIN, F., MAUZAC, M., and RICHARD, H., 1990, *Macromolek. Chem.*, **191**, 1383.
- [12] NOIREZ, L., COTTON, J. P., HARDOUIN, F., KELLER, P., MOUSSA, F., PÉPY, G., and STRAZIELLE, C., 1988, *Macromolecules*, **21**, 2889.
- [13] MOUSSA, F., COTTON, J. P., HARDOUIN, F., KELLER, P., LAMBERT, M., PÉPY, G., MAUZAC, M., and RICHARD, H., 1987, *J. Phys., France*, **48**, 1079.
- [14] NOIREZ, L., KELLER, P., DAVIDSON, P., HARDOUIN, F., and COTTON, J. P., 1988, *J. Phys., France*, **49**, 1993.
- [15] (a) DAVIDSON, P., and LEVELUT, A. M., 1992, *Liq. Crystals*, **11**, 469. (b) DAVIDSON, P., NOIREZ, L., COTTON, J. P., and KELLER, P., 1991, *Liq. Crystals*, **10**, 111.
- [16] GUBINA, T. I., KISE, S., KOSTROMIN, S. G., TALROZE, R. V., SHIBAIEV, V. P., and PLATE, N. A., 1989, *Liq. Crystals*, **4**, 197.
- [17] MAUZAC, M., HARDOUIN, F., RICHARD, H., ACHARD, M. F., SIGAUD, G., and GASPAROUX, H., 1986, *Eur. Polym. J.*, **22**, 137.
- [18] DONALD, A. M., and WINDLE, A. M., 1992, *Liquid Crystalline Polymers* (Cambridge University Press).
- [19] VASILENKO, S., SHIBAIEV, V. P., and KHOKHLOV, A. R., 1985, *Makromolek. Chem.*, **186**, 1951.
- [20] WANG, X. J., and WARNER, M., 1987, *J. Phys. A*, **20**, 549.
- [21] RENZ, W., 1988, *Molec. Crystals liq. Crystals*, **155**, 549.
- [22] MATTOUSI, H., and OBER, R., 1990, *Macromolecules*, **23**, 1809.
- [23] MITCHELL, G. R., COULTER, M., DAVIS, F. J., and GUO, W., 1992, *J. Phys. II, France*, **2**, 1121.
- [24] OHM, H. G., KIRSTE, R. G., and OBERTHÜR, R. C., 1988, *Makromolek. Chem.*, **116**, 1387.
- [25] NOIREZ, L., DAVIDSON, P., SCHWARZ, W., and PÉPY, G., 1994, *Liq. Crystals*, **16**, 1081.
- [26] STRAZIELLE, C., and WEILL, G., *Techniques de l'Ingénieur*, Chapter: 'Diffusion de la lumière', p. 1065-1.
- [27] (a) SCHULTZ, G. V., 1935, *Z. phys. Chem. B*, **30**, 379. (b) FLORY, P. J., 1936, *J. Am. chem. Soc.*, **58**, 1877. (c) SCHULZ, G. V., 1939, *Z. phys. Chem. B*, **43**, 25. (d) ZIMM, B. H., 1948, *J. chem. Phys.*, **16**, 1099.
- [28] For this type of calculation see for example NOIREZ, L., 1989, Ph.D. Thesis, Université d'Orsay, pp. 63-68.
- [29] RIEGER, J., 1988, *J. Phys., Paris*, **49**, 1615.
- [30] RENZ, W., and WARNER, M., 1986, *Phys. Rev. Lett.*, **56**, 1268.
- [31] BROCHARD, F., 1973, *J. Phys., France*, **34**, 411.
- [32] DE GENNES, P. G., *The Physics of Liquid Crystals* (Oxford University Press).
- [33] NOIREZ, L., PÉPY, G., KELLER, G., and BENGUIGUI, L., 1991, *J. Phys. II, France*, **1**, 821.
- [34] (a) JANNINK, G., and DES CLOIZEAUX, J., 1987, *Polymères en solution*, Appendice E. (b) HOCQUART, R., ULP Strasbourg (private communication).
- [35] (a) LAPP, A., 1987, Ph.D. Thesis, Strasbourg. (b) LAPP, A., PICOT, C., and BENOÎT, H., 1985, *Macromolecules*, **18**, 2437.
- [36] DELOCHE, B., 1978, Ph.D. Thesis, Université d'Orsay.